Jambrina-Enríquez, M., Sachse, D., Valero-Garcés, B. L. (2016): A deglaciation and Holocene biomarker-based reconstruction of climate and environmental variability in NW Iberian Peninsula: the Sanabria Lake sequence. - Journal of Paleolimnology, 56, 1, 49-66.

https://doi.org/10.1007/s10933-016-9890-6

A deglaciation and Holocene biomarker-based reconstruction of climate and environmental variability in NW Iberian Peninsula: the Sanabria Lake sequence

Margarita Jambrina-Enríquez[1*]; Dirk Sachse[2,3], Blas L. Valero Garcés[4]

[1] *Departamento de Geología, Facultad de Ciencias, Universidad de Salamanca, Plaza de los Caídos, s/n, 37008 Salamanca, Spain*

[2] *Institut für Erd- und Umweltwissenschaften, Universität Potsdam, Golm-Potsdam, Germany*

[3] *Section 5.1: Geomorphology and Geoecology, Organic Surface Geochemistry Lab, GFZ - German Research Centre for Geosciences, Telegrafenberg, 14473 Potsdam, Germany*

[4] *Instituto Pirenaico de Ecología (CSIC), Avda. Montañana 1005, 50059 Zaragoza, Spain*

* e-mail: margajambrina@usal.es

Joournal of Paleolimnology V.56, pages 49-66 (2016)

Abstract

The molecular biomarker composition of two sediment cores from Sanabria Lake (NW

Iberian Peninsula) and a survey of modern plants in the watershed provide a reconstruction of past vegetation and landscape dynamics since deglaciation. During a proglacial stage in Lake Sanabria (prior to 14.7 cal ka BP), very low biomarker concentration and carbon preference index (CPI) values ∼1 suggest that the *n*- alkanes could have derived from eroded ancient sediment sources or older organic matter with high degree of maturity. During the Late glacial (14.7–11.7 cal ka BP) and the Holocene (last 11.7 cal ka BP) intervals with higher biomarker and triterpenoid concentrations (high %nC$_{29}$, nC$_{31}$ alkanes), higher CPI and average carbon length (ACL), and lower P_{aq} (proportion of aquatic plants) are indicative of major contribution of vascular land plants from a more forested watershed (e.g. Mid Holocene period 7.0–4.0 cal ka BP). Lower biomar- ker concentrations (high %nC$_{27}$ alkanes), CPI and ACL values responded to short phases with decreased allochthonous contribution into the lake that corre- spond to centennial-scale periods of regional forest decline (e.g. 4–3 ka BP, Roman deforestation after 2.0 ka, and some phases of the LIA, seventeenth– nineteenth centuries). Human activities in the watershed were significant during early medieval times (1.3–1.0 cal ka BP) and since 1960 CE, in both cases associated with relatively higher productivity stages in the lake (lower biomarker and triterpenoid concentrations, high %nC$_{23}$ and %nC$_{31}$ respectively, lower ACL and CPI values and higher P_{aq}). The lipid composition of Sanabria Lake sediments indicates a major allochthonous (watershed-derived) contribution to the organic matter budget since deglaciation, and a dominant oligotrophic status during the lake history. The study constrains the climate and anthropogenic forcings and watershed versus lake sources in organic matter accumulation processes and helps to design conservation and management policies in mountain, oligotrophic lakes.

Keywords: Plant n-alkanes, Lipid biomarker, Sanabria Lake, *n*-Alkanes, Holocene, Lateglacial, Iberian Peninsula

Introduction

The analysis of biomarker compounds has been successfully used to reconstruct past climate and environmental variability in association with other geochemical and biological proxies (isotopic and elemental analyses, pollen, macroscopic remains…) in peat (Ficken et al. 1998; Ortiz et al. 2010a, b) and in lake sediments (Brincat et al. 2000; Schwark et al. 2002; Ortiz et al. 2013). Whereas bulk organic matter analyses (elemental or stable composition) give information about general characteristics of sedimentary organic matter, biological markers found in the lipid fraction of sedimentary organic matter (OM) provide more detailed information about the source, production and preservation of OM, and the trophic status of the lakes (Meyers and Ishiwatari 1993; Meyers 2003). Lipid markers have the advantage that they are characteristic of a specific biotic source (vascular land plants, aquatic macrophytes, algae and bacteria), and preserve that information after burial (Rieley et al. 1991; Ficken et al. 1998, 2000). Epicuticular plant waxes consist mainly of aliphatic compounds of higher molecular weight (*n*-alkanes, *n*- alkanols, *n*-alkanoic acids) (Eglinton and Hamilton 1967; Diefendorf et al. 2011; Bush and McInerney 2013). *n*-Alkanes are the most abundant biomarkers applied to paleolimnological reconstructions because their low susceptibility to microbial degradation compared with other geolipids (Volkman et al. 1998), although *n*-alkanoic acids and *n*-alkanols have been included in several studies of lipids in sedimen- tary records.

Sanabria Lake (NW Iberian Peninsula) has proven to be a sensitive area to short-term climatic shifts during the Late Glacial and the Holocene with a strong control of North

Atlantic dynamics (Luque and Julia` 2002; Luque 2003; Julia` and Luque 2006; Julia` et al. 2007; Giralt et al. 2011; Jambrina-Enr´ıquez et al. 2014). Millennial-scale changes in vegetation cover since deglaciation at a local and regional scales have been described in several pollen sequences (Allen et al. 1996; Muñoz-Sobrino et al. 2004, 2007, 2013; Julia` et al. 2007). A recent multi-proxy study (sedi- mentology, physical properties, geochemical compo- sition and diatom assemblages) (Jambrina-Enríquez et al. 2014) reconstructed the evolution of Sanabria Lake and characterized a proglacial stage prior to 13.9 cal ka BP (unit III), followed by deposition of glaciolacustrine sediments until 11.2 ka BP (unit II) and lacustrine sedimentation afterwards (unit I). Landscape dynamics during the Holocene were investigated through facies analyses (flood layers) and geochemical proxies and several phases were identified. In this study, lipid biomarkers (alkanes, alkanols, alkanoic acids and higher plant biomarkers) were determined in the same composite sediment sequence of Sanabria Lake (Jambrina-Enríquez et al. 2014) and in modern plants to assess how watershed (climate, sediment delivery, vegetation evolution, human impact) and lake processes (bioproductivity) have controlled organic matter deposition in Lake Sanabria since the onset of deglaciation.

Study site

Sanabria Lake (42º07'30"N, 06°43'00"W; 1000 m a.s.l.) (Fig. 1a) is the largest lake of glacial origin in the Iberian Peninsula (368 ha). The lake has an elongated morphology along a W-E direction with two over excavated sub-basins (of 51—eastern- and 45 m—western- maximum depth) separated by a ridge located 20 m below the water surface (Vega et al. 2005) (Fig. 1b).

The lake is located in an exoreic drainage basin (127.3 km^2) in the eastern foothill of the

Segundera Range (2127 m a.s.l.), closed by a terminal moraine (Vega et al. 2005) (Fig. 1c). The bedrock consists of granitic rocks (*Ollo de Sapo* gneis and granodiorite), locally covered by Quaternary glacial deposits (Rodríguez- Rodríguez et al. 2011) (Fig. 1d). The Tera River is the main inflow (about 85 % water flow) and the only surface outflow of the lake, with higher flows between October and April (Giralt et al. 2011). The region has a continental climate with Atlantic influences (the North Atlantic Oscillation exerts a strong influence particularly in winter precipitation, Trigo et al. 2004), with annual precipitation about 1465 mm and mean annual temperature about 10°C (Ribadelago—1000 m a.s.l.—weather station; data supplied by Vega JC, from the Laboratorio Limnológico Lago de Sanabria, JCyL). The watershed vegetation consists of shrubs and pastures in the highplains, a *Quercus pyrenaica* woodland with patches of *Pinus sylvestris* L.—which at present are repopulations—*Juniperus oxycedrus* L., *Taxus baccata* L. and *Ilex aquifolium* L. between 1700 and 1500 m a.s.l., and a *Quercus pyrenaica* forest below 1500 m a.s.l (Vega et al. 1992; Julià et al. 2007). Around the lake, the vegetation includes *Populus nigra* L., *Alnus glutinosa* (L.) Gaertn, *Fraxinus angustifolia* Vahl. and *Salix salviifolia* Brot. Macrophytes are well developed in the littoral zone (*Equisetum fluviatile* L., *Potamogeton natans* L., *Utricularia australis* R. Br., *Myriophyllum alterniflorum* DC., *Isoetes velatum* A. Braun, *Nitella flexilis* (L.) Agardh, *Eleocharis palustris* (L.) Roem. and Schultes, *Fontinalis antipyretica* Hedw. and *Carex vesicaria* L. (Vega et al. 1992; García et al. 1992; Julià et al. 2007). Managed pastures are common in the nearby Ribadelago Nuevo and San Martín de Castañeda villages (Fig. 1e).

Sanabria Lake is a warm, oligotrophic and monomictic lake, thermally stratified from March/April to November/December. The lake water is calcium-bicarbonate dominated (Ca^{2+} >Na^{+} >Mg^{2+} > K+ and HCO^{-3} > Cl^{-} > SO_4^{2-}), with

very low ion concentration (conductivity between 14.5 and 14.9 µS cm^{-1} and the total solids dissolved between 7.5 and 13.0 mg L-1), slightly acidic (pH between 6.2 and 6.5), and with low alkalinity (average 0.045 meq L^{-1}). The water residence time is about 5–9 months, and the whole water column is oxygenated throughout the year (de Hoyos 1996). The limnological variability is primarily controlled by fluctuations in the seasonal precipitation and wind, and the main Atmospheric Circulation Mode associated with the winter limnological processes are the North Atlantic Oscillation (NAO) and the Scandinavian (SCAND) patterns modes, whereas only the East Atlantic (EA) mode weakly influences some processes during the summer (Herna´ndez et al. 2015)

Materials and methods

Modern vegetation sampling

In order to determine the *n*-alkane distributions of possible modern OM sources to Sanabria Lake sediments, eight plant species were chosen for leaf wax lipid analyses based on their relatively high abundance in the watershed and on the lakeshore. Samples of the most common terrestrial species were collected during September 2010: *Quercus pyrenaica* as the dominant tree specie and *Alnus glutinosa* and *Fraxinus angustifolia* as abundant trees, and shrubs (*Juniperus* spp.) and herbs (*Pteridium aquilinum* (L.) Kuhn) along the lake margins. Submerged/floating (*Myriophyllum alterniflorum*) and emergent macrophytes (*Eleocharis palustris, Equisetum fluviatile*) were sampled in June 2010.

Lipid extraction

The Sanabria Lake composite sequence used in this study is composed of a long (8.9 m) (SAN04-3A-1K) and a short (64 cm) core (SAN07-2M) retrieved from the deepest

148 sub-basin (eastern sub-basin, Zmax = 51 m) in 2004 and 2007 respectively (Fig. 1b).
149 Forty eight sediment samples from core 3A (1-cm-thick sample about every 15 cm) and
150 twelve samples from core 2M (1- cm-thick sample about every 5-cm) were analyzed.
151 The selected sixty sediment samples were selected as representatives of the three units
152 previously defined in the same cores by Jambrina-Enríquez et al. 2014. The chronology
153 for this sequence is based on 14 ^{14}C AMS dates, $^{210}Pb/^{137}Cs$ techniques and the
154 identification of the 1959 CE clastic horizon associated with the catastrophic breach of
155 the Vega de Tera Dam (Jambrina-Enríquez et al. 2014; Fig. 2).
156 Plant leaf samples were freeze-dried using a cryogenic mill (6770 Freezer/Mill®) to
157 obtain between 0.5 and 1 g of ground leaves. Depending on total organic content, 1–2
158 g of wet sediment samples were dried, ground and homogenized.
159 The *n*-alkane, *n*-alkanol and *n*-alkanoic acid identification and quantification were
160 carried out at the Biomarker laboratory of the Institute for Earth- and Environmental
161 Sciences at University of Potsdam, Germany. Soluble organic matter in sediment
162 samples was extracted using an accelerated solvent extractor ASE 350 (Dionex) with
163 a dichloromethane/methanol mixture (9:1) at 100 °C and 1500 psi for 5 min in 3 cycles.
164 Lipids from plant leaf samples were extracted in 30 mL 9:1 dichloromethane/methanol
165 using a sonicator and then the mixture was filtered. The total lipid extracts were
166 evaporated and redissolved in 1.5 mL n-hexane.
167 After addition of internal standard (5α-androstane, 5 µg) the total extract (containing
168 free lipids) was separated using solid phase extraction (SPE) on a silica gel column
169 chromatography (2 g silica per column, 0.040–0.063 mesh, Alfa Aesar) previously
170 cleaned with n-hexane into three fractions of different polarity, namely an alkane
171 fraction (F1, eluted with 20 mL n-hexane), an alcohol fraction (F2, 20 mL DCM) and
172 a alkanoic acid fraction (F3, 15 mL DCM/ MeOH, 2:1). Before SPE, the silica gel was

heated to 450 °C for 10 h and deactivated using 5 % w/w of ultrapure water. After addition of internal standard 5a-androstan-3ß-ol (5 µg), F2 and F3 were derivatized by heating the DCM dissolved fractions at 80 °C for 30 min with the addition of 50 lL of bis-(trimethylsi- lyl) trifluoroacetamide (BSTFA). The eluent was evaporated to dryness and re-dissolved DCM.

The three fractions were identified and quantified by gas chromatography with a coupled flame ionisation detection and mass-selective detector (GC–FID/ MSD Agilent 7890A GC-5975C MSD) equipped with a HP–5MS capillary column (29.8 m, ID: 250 µm, film thickness 0.25-µm). The GC was programmed to an initial temperature of 70 °C for 2 min, a heating rate of 12 °C min^{-1} to 140 °C and a final temperature of 320 °C for 15 min, with Helium as the carrier gas. The PTV injector was held at a split ratio of 5:1 at an initial temperature of 70 °C. With injection, the injector was heated to 300 °C at a programmed rate of 720 °C min^{-1} and held at this temperature for 2.5 min. The compounds were identified by comparison of their retention times and mass spectra with those of reference compounds. Quantification was based by comparison of peak areas with those of known quantities of standards: 5α-androstane (5 µg) and 5α-androstan-3ß-ol (5 µg) added to the samples after and before the extraction respectively. The n-alkane, n-alkanol and n-alkanoic acid concentrations are expressed as lg of individual compound per gram of dry sample (µg gds^{-1}).

Results

Modern vegetation

The biomarker distributions varied slightly between species and showed mainly unimodal patterns (Table 1). The submerged/floating macrophyte (*Myriophyllum alterniflorum*), dominated by nC_{27}-alkane, shows the lowest n-alkane concentration (8.7 µg gds^{-1}).

198 Emergent aquatic plants (*Eleocharis palustris, Equisetum fluviatile*), shoreline plants
199 (*Pteridium aquilinum*) and trees (*Alnus glutinosa, Fraxinus angustifolia*) were dominated
200 by nC_{29}-alkanes and relatively with low contributions from other chain-length
201 homologues. *Quercus pyrenaica* and *Juniperus* spp. trees showed the highest n-alkane
202 concentration (4.2 mg gds^{-1} and 3.8 mg gds^{-1} respectively) dominating long chain
203 homologues at nC_{31}. Upland terrestrial plants were mainly dominated by nC_{18}-alkanoic
204 acid, and macrophytes and shoreline plants by nC_{16} (carbon number maximum—Cmax).
205 The alkanol distribution does not show a clear pattern.
206 Biogenic molecular markers including triterpenes and terpenoids were also identified in
207 the leaf samples. Phytol and phytosterols (i.e. β-sitosterol and lupeol) were identified in
208 fraction 3 but only β-sitosterol was detected in all samples, although in variable
209 abundance (Table 1). Ursolic acid (3beta-Hydroxy-Urs-12-en-28-oic acid) was the most
210 abundant triterpenoid (e.g. *Juniperus*, 9.5 mg gds^{-1}, *Fraxinus*, 789.9 µg gds^{-1}, *Quercus*,
211 31.4 µg gds^{-1}) while friedelin was identified only in *Quercus* (13.1 µg gds^{-1}).
212
213 ***The Sanabria sequence***
214 *n-Alkane distribution and concentration in lake sediments*
215 n-Alkanes were always dominated by mid- to long carbon chain lengths with a strong
216 odd/even carbón number preference. The most abundant homologues were
217 $nC_{27}+nC_{29}+nC_{31}+nC_{33}$, except for one sample at 32 cm depth (3A core), which was
218 dominated by $nC_{21}+nC_{23}+nC_{25}$. The lowest concentration was found in unit 3 and 1A
219 (core 3A), and the highest in subunit 1A (core 2M). Unit 3 mainly shows a unimodal
220 distribution maximizing at nC_{31} except for some samples with peak amounts of nC_{22}.
221 Subunit 2C is characterized by a unimodal distribution maximizing at nC_{31}, whereas
222 subunits 2B and 2A show a unimodal pattern with major variability (nC_{27}, nC_{29} or nC_{31}).

Unit 1 was characterized by three different patterns: (1) single peak distribution dominated by nC_{27} or nC_{29} (subunit 1E), (2) double peak distribution dominated by nC_{27} and nC_{31} (subunits 1D and 1C) alternating with a single peaks distribution maximizing at nC_{27}, nC_{29} or nC_{31}, and (3) a single peak distribution dominated by nC_{31} (subunit 1B). Subunit 1A has a relatively high concentration of nC_{23} (core 3A) and nC_{31} (core 2M) (ESM1).

To evaluate the distribution of n-alkanes we used the carbon preference index—CPI (1), Average Carbon Length—ACL (2) and the Proportion of aquatic plants—Paq (3) (ESM1):

$$CPI_{21–33\text{-alkane}}: \text{odd}\sum[C21–33]/\text{even}\sum[C22–32] \quad (1)$$

$$ACL_{21\text{-}33}: \sum(Ci * [Ci])/\sum[Ci].\ 21 < i < 33. \quad (2)$$

$$P_{aq}: (C_{23} + C_{25})/(C_{23+25+29+31}) \quad (3)$$

The ranges of CPI, ACL and Paq vary from 0.9 to 14.0, from 25.4 to 29.8 and from 0.1 to 0.6, respectively. The highest CPI and ACL, and lowest Paq values were mainly associated with higher n-alkane concentrations (higher nC_{29} or nC_{31}); lower CPI and ACL, and higher Paq values correspond with lower nalkane concentrations (ESM1).

n-Alkanols

The distribution of n-alkanols ranges from nC_{20} to nC_{34} and even carbon numbered homologues predomínate (ESM2). The total n-alkanol concentration varies between 9.0 and 584.4 µg gds^{-1} with a similar pattern as the total n-alkane content. Lower values occur in units 3 (24.6 µg gds^{-1} mean value) and 1A (15.4 µg gds^{-1} mean value) and higher in subunits 1D (55.5 µg gds^{-1} mean value) and 2C (60.0 µg gds^{-1} mean value). The n-alkanols showed a unimodal distribution with a maximum at nC_{26}, nC_{28}, or nC_{30} (nC_{28} is dominant in units 3, 2 and 1E, and nC_{26} in subunits 1B and 1A) and a bimodal distribution with maximum at nC_{26} and nC_{28} (subunits 1E, 1D and 1C) (ESM2). CPI-alkanol (4)

varied over a wide range (0.1–80.3) and show major fluctuations in basal units 3 and 2, whereas similar values occur in unit 1 (ESM2):

$$CPI_{20-34} = even\sum[C20–34]/odd\sum[C21–33] \quad (4)$$

Higher (lower) values are mainly related to higher (lower) total n-alkanol concentrations.

n-Alkanoic acids

The n-alkanoic acid distribution was in the range from C_{16} to C_{32} with even carbon numbered compounds predominating over the odd carbon numbered homologues (ESM2). The total n-alkanoic acid concentration varied between 3.1 and 641.6 µg gds^{-1} and showed a similar pattern as total n-alkane and n-alkanol contents. Lower values appear in unit 3 (9.2 µg gds^{-1} mean value) and higher in subunit 1D (110.7 µg gds^{-1} mean value). The n-alkanoic acid distribution showed a unimodal distribution with maxima at nC_{24}, nC_{26} or nC_{28} and a bimodal distribution (nC_{26}+nC_{28}). Unit 3 showed a bimodal distribution maximizing at nC_{22} and nC_{24} (ESM2). CPI-acid (5) values ranges from 0.8 to 16.5 (ESM2):

$$CPI_{16-32} = even\sum[C16–32]/odd\sum[C17–31] \quad (5)$$

Higher (lower) values mainly correspond with the higher (lower) total n-alkanoic concentrations, with a pattern similar to the CPI-alkanol.

Triterpenoids: higher plant biomarkers

Several higher plant derived triterpenoids were identified in the sediments, particularly β-sitosterol in the alkanol fraction, and friedelin and ursolic acid in the alkanoic acid fraction. The concentration of friedelin, β-sitosterol and ursolic acid ranged from 0.2 to 34.2 µg gds^{-1}, from 0.5 to 14.1 µg gds^{-1} and from 0.1 to 79.5 µg gds^{-1} respectively, with high total biomarker values in subunit 1D and low in unit 3 and 1A. The highest (lowest)

biomarker concentrations coincide with the highest (lowest) values of total nalkane, n-alkanol and n-alkanoic acid concentrations (ESM1).

Discussion

Biolipids in modern vegetation

Terrestrial upland and shoreline plants can be assumed to be the dominant source of the more abundant mid/long chain length n-alkane homologues (nC_{27}–nC_{35}) in the lake sediments (Table 1, Fig. 3). Although the nC_{31}-alkane occurred in high abundance in *Quercus* and *Juniperus* (higher ACL), it was also found as a secondary component in *Alnus glutinosa* (lower ACL). nC_{27}-Alkane is more abundant in the submerged aquatic plants *Myriophyllum alterniflorum* (lower ACL). However, both mid- and longer chain length homologues can be traced to aquatic and terrestrial sources (Fig. 3a). The ACL values of woody and non-woody plants are similar (Table 1). ACL values for alkanes in modern plants from around the world reported by Bush and McInerney (2013) and Wang et al. (2015) do not show a significant difference between these two main types of plants. Although the fundamental assumption for using ACL as proxy for vegetation dynamics is that woody plants produce leaf waxes with shorter ACL values than non-woody plants (Cranwell 1973), considerable caution is necessary in using ACL values as a proxy indicator of past changes in vegetation, environment and climate since environmental and plant physiological factors could influence on ACL values (Wang et al. 2015). The long-chain fatty acid nC_{26} was dominant in upland terrestrial plants and nC_{28} in macrophytes and shoreline plants.

The nC_{30}-alkanoic acid was found in higher abundance in *Juniperus* whereas *Quercus*, *Fraxinus* and *Alnus* showed higher content of nC_{26} (Fig. 3b). The nC_{30}-alkanol occurred in higher values in *Juniperus* and *Fraxinus* whereas nC_{28} and nC_{26} dominated in *Alnus*

and *Quercus* respectively (Fig. 3c). 'β-sitosterol', identified in higher abundance in *Fraxinus*, has been reported as a biomarker of higher plant input and marsh grasses (Canuel et al. 1997); however, it was also identified in algae and cyanobacteria (Volkman et al. 1999; Rontani and Volkman 2005). Ursolic acid and friedelin (assumed to be derived from angiosperms, Simoneit 1986; Otto and Simoneit 2001) were identified in higher concentrations in *Juniperus* and *Quercus* respectively.

Quercus woodland is dominant in the drainage área of Sanabria Lake, with local presence of *Alnus* and *Fraxinus* around the lake, whereas *Juniper* woodland is dominant above 1500 m a.s.l. (Julià et al. 2007), with patches of *Juniperus* in shaded and protected areas. These data suggest that deciduous *Quercus* and conifer *Juniperus* leaves could be major contributors of n-alkanes into lake sediments, with a minor influence by *Fraxinus* leaves, and a negligible input of leaves from *Alnus.*

The Sanabria Lake biolipid record: environmental and climate implications

The distribution of the different leaf wax n-alkane homologues in the Sanabria Lake sediments, a comparison with their distribution in present-day vegetation (Fig. 3) and the information from local pollen sequences (Allen et al. 1996; Muñoz-Sobrino et al. 2004, 2007, 2013; Julià et al. 2007) (Figs. 4, 5), help to reconstruct changes in terrestrial plant input, with the assumption that the n-alkane distributions of modern plant species are representative of past plant assemblages (Schwark et al. 2002). However, we have to take into account that several plant species have similar alkane composition (Eglinton and Hamilton 1967; Rieley et al. 1991) and that the abundance and/or chain-length composition of leaf-waxes can change in response to environmental stress or during leaf ontogeny (Shepherd and Griffiths 2006; van Maarseveen et al. 2009).

A number of indices calculated using n-alkane abundance as ACL, Paq, and CPI allow discrimination of the OM sources in the sediment (Fig. 6). The ACL index responds to changes in vegetation, but individual plants can also change their n-alkane distributions as a reaction to temperature and hydrological variations (Sachse et al. 2006; Hoffmann et al. 2013). The Paq index reflects the relative contribution of emergent (values 0.1–0.4), submerged/floating aquatic macrophytes (values >0.4) and terrestrial (values <0.1) plants (Ficken et al. 2000). The n-alkanes from the cuticular wax of higher plants have a strong odd predominance and CPI values>5 whereas n-alkanes from bacteria and algae have low CPI values of ca 1 (Cranwell et al. 1987). Degradation of sediment organic matter may account for systematically changing n-alkane ratios such as the CPI, $Alk_{>C25}/Alk_{<C25}$ and long-chain n-alkane ratios [LARs: $C_{27}/(C_{27} + C_{31})$, $C_{29}/(C_{31} + C_{29})$, $C_{27}/(C_{27} + C_{29})$] (Buggle et al. 2010; Zech et al. 2012). High CPI from modern soils and peatbogs results from slow microbial degradation and diagenesis under cold/dry climate, whereas low CPI results from higher microbial degradation under warm/wet conditions (e.g. Roñanzas peatbog-NW Iberia, Ortiz et al. 2010a). However, higher CPI has been evidenced during warm periods (e.g. Lake Baikal, Brincat et al. 2000), and also a North to South European transect in lake surface sediments reflects an increase in CPI values from cold to warm regions (Sachse et al. 2004).

Biomarker composition in Sanabria Lake sequence is characterized by higher abundance of long-chain nalkanes (nC_{27}, nC_{29}, nC_{31}) with a distinct odd-over even distribution, and long-chain n-alkanol (nC_{20}–nC_{34}) and n-alkanoic acid (nC_{26}–nC_{28}), both with a distinct even-over-odd distribution. This reflects a dominant terrestrial land plant input highly dependent of sediment delivery and wathersed vegetation. Such a biomarker distribution is typical of oligotrophic freshwater lakes (Cranwell and Volkman 1981; Kawamura and Ishiwatari 1985). The positive relationship between friedelin, β-sitosterol and ursolic acid

concentrations with the total lipid content in the sediment (r = 0.83, 0.90 and 0.83 respectively) suggests that intervals of higher biomarker concentrations, higher CPI and ACL values present greater contributions from vascular plants. Lower biomarker concentrations and CPI and ACL values occurred in two types of sediment intervals: (1) short phases with decreased allochthonous contribution into the lake that seem to correspond to centennial-scale periods of less forested watershed and (2) flood events that represent rapid deposition dominated by clastic sediments.

In the following section, we compare the biolipid record with local reconstructions of fluvial activity (last 14 ka, Jambrina-Enríquez et al. 2014), temperature (15.6 and 10.5 cal ka BP, La Roya, Muñoz-Sobrino et al. 2013), and vegetation dynamics (Allen et al. 1996; Muñoz-Sobrino et al. 2004, 2007, 2013; Julià et al. 2007). The good correspondence with other independent reconstructions suggests that biolipid record reflect changes in the lake-watershed system and not post-depositional processes (Fig. 6).

A proglacial environment (GS-3-2, prior to 14.6 cal ka BP).

Low total lipid contents and TOC values reveal low OM input and/or greater degradation of organic compound during deglaciation (unit 3, prior to 14.6 cal ka BP). Depositional processes were strongly controlled by the melting glaciers, as reflected by the sedimentation of massive silts with sand pockets with high magnetic susceptibility and very low organic matter content (Jambrina-Enríquez et al. 2014; Borruel-Abadía et al. 2015). The low triterpenoid concentrations (friedelin is the only terrestrial biomarker detected with concentrations below 2 lg gds-1), ACL (25.0–27.0), and Paq index (C0.4) reflect the presence of OM derived mainly from aquatic plants (Hedges and Prahl 1993). Low CPI (~1) and $Alk_{>C25}/Alk_{<C25}$values, the LAR ratios covarying with the CPI and a

unimodal n-alkane distribution maximizing at nC_{22} (ESM1), reflects intensive n-alkane degradation and low production (Fig. 6). Degradation of these lipids is suggested by the decrease in fatty acid concentrations, more subject to be attacked than are n-alkanes.

A recent study of the compound-specific radiocarbon age of plant waxes in lake sediments showed that biomarkers can have a long residence time in soils (Douglas et al. 2014). This may lead to the export of terrigenous carbon derived from material of different ages or compounds originated from eroded ancient sediment sources (Mazurek and Simoneit 1984; Hedges and Prahl 1993; Meyers 2003). Pollen records from nearby sites as Lleguna (Muñoz-Sobrino et al.2004, previously named Sanabria marsh by Allen et al. 1996) and Laguna de las Sanguijuelas (Muñoz-Sobrino et al. 2004) show a steppic landscape. The increasing upward trend in ACL, total biomarker and organic content, and the change in the n-alkane distribution (high $\%nC_{31}$) could reflect the increase in shrubs and trees in the watershed as deglaciation progresses around 16.3–15.1 cal ka BP (Muñoz-Sobrino et al. 2004, 2007).

The GI-1 interstadial (Bølling–Allerød,14.6–13.0 cal ka BP)

The TOC and biomarker concentration increase indicates higher OM input and/or improved preservation of organic compounds during the GI-1 interstadial (unit 3 and subunit 2C, 14.6–13.0 cal ka BP). During this period, the Tera glacier retreated from the lake basin into higher altitude areas of the watershed, and influenced less the lake depositional dynamics (Jambrina-Enríquez et al. 2014; Borruel-Abadía et al. 2015). High CPI and $Alk_{>C25}/Alk_{<C25}$ values and LAR ratios point to minimal microbial degradation of OM. In spite of an increase in bioproductivity in the lake (Jambrina-Enríquez et al. 2014), the predominant unimodal n-alkane distribution (high $\%nC_{31}$), the high ACL (27.5–29.4) and CPI-alkane values (1.8–9.0) and low Paq index profile (0.1–0.3) suggest

398 that most of the OM deposited in the lake was still of terrestrial origin with low
399 contribution of aquatic macrophytes (Ficken et al. 2000; Meyers 2003). According to the
400 distribution of long-chain nalkane in the sediment and comparison with distribution in
401 present-day vegetation (Fig. 3a), oak and juniper would be expected to be the main
402 producers of nC_{31}-alkane. The predominance of friedelin and bsitosterol concentrations
403 (terrestrial biomarker from *Quercus*) over ursolic acid concentration (terrestrial
404 biomarker from *Juniperus*) (Table 1) would point to *Quercus* as the dominant species in
405 the forest. Local pollen sequences show a large variability of forest composition
406 depending on altitude (Munñoz-Sobrino et al. 2004, 2007). In the highlands (La Roya),
407 pine and oak woodlands developed from 14.5 to 12.5 cal ka BP (Muñoz-Sobrino et al.
408 2013) while *Juniperus* increased in Sanabria marsh with some evidence of *Quercus*
409 development (Allen et al. 1996) (Fig. 4). However a *Quercus* phase has been identified
410 in the nearby Laguna de Las Sanguijuelas (ca. 14,000 and 13,600 cal BP) and in Lleguna
411 (ca. 13,600 and 13,000 cal BP) (Muñoz-Sobrino et al. 2004, 2007) and could correspond
412 with the friedelin peak (7.2 lg gds-1) at ca. 13,300 cal BP.
413
414 *GS-1/Younger Dryas-YD (13.0–11.7 cal ka BP)*
415 A significant decrease in total biomarker concentration, terrestrial biomarkers content and
416 TOC values and changes in biolipid composition (low CPI and $Alk_{>C25}/Alk_{<C25}$ values
417 and high LAR ratios) indicate changes in the watershed vegetation (reduced forest cover)
418 and sedimentation patterns (glacier advances) synchronous to GS-1. Low ACL (27.5) and
419 high Paq (0.3) could suggest an increase in aquatic macrophytes (Ficken et al. 2000). The
420 atomic C/N values (~15) during the B/A-YD transition (subunit 2B, 13.0–12.4 cal ka BP)
421 did not show a significant change, pointing to a reduced contribution of terrestrial land
422 plants (high $\%nC_{27}$) (Fig. 4), coherent with pollen records as Laguna de las Sanguijuelas,

423 revealing a landscape characterized by *Artemisia–Graminae* (Muñoz-Sobrino et al.
424 2004). However, some periods with higher OM from land plants occurred, as the one
425 recorded at 12.7 cal ka BP. The occurrence of some forest increase phases—pine and oak
426 woodlands before 12.5 ka in La Roya (Muñoz-Sobrino et al. 2013) and Lleguna (Muñoz-
427 Sobrino et al. 2007) would fit with the identified intervals with higher total biomarker and
428 friedelin contents (higher %nC_{31}-alkane, longer-chain n-alkanes increase, shorter-
429 chainalkanes decrease, higher CPI and ACL) (Figs. 4, 6). Considering the modern plant
430 n-alkane and n-alkanol distributions, alder (*Alnus glutinosa*) could have been responsible
431 for the high relative abundances of nC_{27}-alkane (and nC_{31}) and nC_{28}-alkanol before 12.4
432 cal ka BP, and oak (*Quercus*) for the high relative abundances of nC_{31}-alkane, friedelin
433 and β-sitosterol at 12.7 cal ka BP.
434 During the YD-Holocene transition (subunit 2A, 12.4–11.7 cal ka BP), decreasing C/N
435 atomic ratio (C/N = 8–11), increasing biogenic silica content (BioSi = 10 %) and a plant
436 community characterized by abundant submerged aquatic plants (*Cyperaceae,*
437 *Myriophyllum, Potamogeton and Nymphaea*) recorded in Lleguna (Muñoz-Sobrino et al.
438 2004) support a dominant aquatic component in organic matter (high %nC_{27}, low ACL
439 and high Paq). These biolipid changes suggest some centennial-scale variability in the
440 watershed-lake system (run-off and/or vegetation cover) in response to changing
441 hydrology. Although the age-resolution of the Sanabria record is relatively low, these
442 internal changes in biomarker composition are coherent with the two-phase internal
443 structure of the Younger Dryas documented in northern (Bakke et al. 2009; Lane et al.
444 2013) and in southern (Bartolomé et al. 2015) Europe.
445
446 *The Early Holocene (11.7–7.5 cal ka BP)*

447 The predominant n-alkane chain (C_{29}), ACL (29.1), CPI (>9.7) and Paq (0.1) values point
448 to higher terrestrial and shoreline species compared to algal input until 11.2 cal ka BP
449 (subunit 2A) and less terrigenous plant input (high %nC_{27}, ACL = 27.6, CPI = 6.5, Paq =
450 0.3) between 11.2 and 10.1 cal ka BP (subunit 1E) (Eglinton and Hamilton 1967; Ficken
451 et al. 2000) (Figs. 4, 6). Warmer and wetter conditions are interpreted from the nearby
452 pollen sequences—Lleguna and Laguna de las Sanguijuelas—as tree pollen increased
453 between 11.8 and 10.2 cal ka BP (Muñoz-Sobrino et al. 2004, 2007).
454 After this initial phase of forest expansion at the Holocene onset, local records show a
455 decrease in tree pollen (Sanabria marsh, Allen et al. 1996), Lleguna and Laguna de las
456 Sanguijuelas (Muñoz-Sobrino et al. 2004, 2007) and an increase of clastic sediment
457 delivery to the lake (Jambrina-Enríquez et al. 2014) (Figs. 4, 6). During the 10–9 cal ka
458 BP period the total lipid concentration decreased, associated with a decline of longer-
459 chain alkanes (high %nC_{27}). The apparent dominance of aquatic vegetation as suggested
460 by the relatively higher Paq and lower ACL is likely a result of the reduction of terrestrial
461 forest vegetation and OM input. This espisode of increased river input shows slightly
462 lower values of $Alk_{>C25}/Alk_{<C25}$ ratio whereas the LAR values are higher.
463 After 9.1 ka (subunit 1E), biomarker content increased (high %nC_{29} and nC_{31}), high CPI
464 and ACL, and low Paq, suggesting a rapid recovery of the abundance of land plants (Fig.
465 6) during a period still dominated by relatively higher clastic input to the lake. Based on
466 modern plant biomarker distribution and pollen sequences, a plant community with
467 abundant *Quercus, Alnus and Fraxinus* would be expected to produce high relative
468 abundances of nC_{29} and nC_{31}-alkanes, nC_{28} and nC_{30}-alkanols, and nC_{26}-alkanoic acid
469 (Fig. 3a).
470
471 *Mid Holocene (7.5–3.7 cal ka BP)*

This period (corresponding to subunits 1E, 1D and 1C) has the highest biomarker concentrations (357.7–542.7 μg gds^{-1}) in the whole sequence (except for a short event in the sixteenth century) (Fig. 4). The relatively high C/N atomic ratio (C/N 13–15), the dominance of ∑n-$C_{27,29,31}$ alkanes and high triterpenoid concentrations (friedelin and ursolic acid are abundant), higher Alk>C25/Alk<C25, ACL (~29), CPI (8–9) and lower Paq (0.1) values reveal a dominant allochthonous (terrestrial plants) OM source (Fig. 6). This is consistent with the maximum regional forest development during the Mid Holocene (Allen et al.1996; Mun˜oz-Sobrino et al. 2004). Lleguna and Laguna de las Sanguijuelas sequences recorded high tree pollen content (~90 %), mixed pine/oak formations, and increasing warmth-demanding taxa (Muñoz-Sobrino et al. 2004). Compared with modern plant biomarker distribution, the mid Holocene plant community would be consistent with abundant *Quercus, Fraxinus and Alnus* (Fig. 3).

Clastic flood layers (Jambrina-Enríquez et al. 2014) are characterized by low biomarker concentrations—at 7.5 ka (117.5 μg gds^{-1}), 5.7 ka (103.4 μg gds^{-1}) and 4.7 ka (91–96 μg gds^{-1})—less abundant longer-chain alkanes (higher %nC_{27}-alkane), low CPI (4–5) and ACL (~27) and high Paq (0.3–0.4) (Figs. 4, 6). Plant waxes occurring within flood layers may be the result of a mixture of waxes derived from soils (terrigenous carbon, e.g. pre-aged vascular-plant-derived with residence times of decades to centuries) and primary productivity. Although it is generally assumed that the different components of a sediment horizon are contemporaneous, dated leaf waxes have produced variably older ages than the sediments as substantial contributions of eroded soil from the catchment may dilute the primary production (Douglas et al. 2014).

Although several oscillations in the abundance of Cyperaceae pollen record short phases of inundation and recovery in Lleguna (Muñoz-Sobrino et al. 2004),we argue that the

observed fluctuations respond to changes in the Tera River delivery more than to changes in the relative development of littoral lake environment (Jambrina-Enríquez et al. 2014).

The Late Holocene (3.7–1.0 cal ka BP)

Biomarker and triterpenoid concentrations decreased along this period (subunit 1C, 1B and 1A) consistent with the regional forest retreat in northwest Iberia since ca. 4000 cal BP, due to a combination of anthropogenic impact (e.g. forest burning for pastures or agriculture) (Allen et al. 1996; Muñoz-Sobrino et al. 2004) and climatic factors (Muñoz-Sobrino et al. 2009; Jambrina-Enríquez et al. 2014). The low abundances of mid and long-chain n-alkanes (high %nC_{31}) and ACL (~28), CPI (5–6) and Paq (0.2–0.3) values (Fig. 4) indicate a mixed input of terrigenous and aquatic plants. The $C_{27}/(C_{27} + C_{31})$, $C_{29}/(C_{31} + C_{29})$ ratios and the CPI show high correlation coefficient (r = 0.7). Atomic C/N values (14–15) and TOC (10 %) are higher except during the 3.7–3.0 cal ka BP period (C/N = 11–12; TOC = ~5 %) with higher river input and clastic sediment delivery to the lake (Jambrina-Enríquez et al. 2014) (Fig. 6).

Intervals of relatively higher biomarker concentrations around 3.0 (219.75 µg gds^{-1}) and 2.0 cal ka BP (366.83 µg gds^{-1}) with high CPI (~6) and ACL (28–29) (high %nC_{31}-alkane) and low Paq (0.1–0.2) represent periods with higher allochthonous OM input to the lake (Figs. 4, 6). Both, modern plant biomarker distribution and pollen records from Sanabria Lake (Luque 2003; Julià et al. 2007) suggest a Late Holocene plant community with abundant *Quercus and Alnus* (Fig. 3). The 3.0 phase correlates with higher magnetic susceptibility values indicative of higher sediment delivery (run off or early deforestation) (Jambrina-Enríquez et al. 2014). Interestingly, the 2.0 cal ka BP interval shows lower magnetic susceptibility values (Jambrina-Enríquez et al. 2014) suggestive of a lower

Roman impact on the landscape, consistent with the absence of a stable and continued Roman settlement in this area (Guijarro-Menéndez 2012).

Particularly interesting is the decrease in the absolute abundance of long-chain n-alkanes and the increase in the relative abundance of mid chain nalkanes (high %nC_{23}) at 1.1 cal ka BP (subunit 1A). Relatively higher C/N atomic ratios (C/N = 14–15) are indicative of stronger terrestrial organic matter input but the lower biomarker and triterpenoid concentrations, ACL (25) and CPI (2.5) values and the higher Paq (0.5) values reflect the development of a more abundant and widespread community of aquatic plants (higher contribution from submerged floating macrophytes) (Fig. 4). This is consistent with a more productive lacustrine ecosystem (Julià et al. 2007; Jambrina-Enrìquez et al. 2014) and higher percentages of aquatic pollen (Allen et al. 1996; Julià et al. 2007) (Fig. 6). A stronger anthropic influence during this period is suspected, as it corresponds with the foundation of the San Juan Bautista monastery in Ribadelago village and likely, the use of the riparian areas of the Tera River for farming and grazing activities, particularly during the eighth and nineth centuries (Guijarro-Menéndez 2012).

The Little Ice Age and the recent changes (1520–2004 CE)

The 1520–1600 CE period (base of 2M short core) corresponds to deposition of organic- and biogenic silica—rich silts with abundant long-chain n-alkanes (high %nC_{31}) and lower mid-chain n-alkanes and the highest Holocene biomarker concentration (200–1500 lg gds-1) (Figs. 5, 6). The high ACL (29–30) and CPI (9–14), and low Paq (0.1) suggest higher contribution from terrestrial plants. Based on modern plant biomarker distributions, a plant community with abundant *Quercus, Alnus* and *Fraxinus* would be expected to produce the observed high abundances of triterpenoids (Fig. 3). This is

544 consistent with the forest recovery documented in Sanabria Lake during the late
545 sixteenth—early seventeenth centuries (Julià et al. 2007).
546 The decrease of biomarker concentrations (lower long and mid-chain n-alkanes, high
547 %nC_{31}), relatively lower ACL (28) and CPI (6), and higher Paq (0.2) values from ca. CE
548 1600 to 1760 corresponds to an interval with higher clastic sediment delivery into the
549 lake, possibly associated with increased run-off and rainfall during the Little Ice Age
550 (Luque 2003; Julià and Luque 2006; Julià et al. 2007; Jambrina-Enríquez et al. 2014) and
551 suggest a decline in terrestrial shoreline species and aquatic plants. The decreasing trend
552 in arboreal pollen from ca. CE 1600 to 1900 (Julia` et al. 2007) is also paralelled by the
553 n-alkane indices.
554 The clastic layer deposited during the flash flood after the Tera River dam collapse in CE
555 1959 shows higher total lipid (about 300 µg gds^{-1}) and terrestrial biomarker content,
556 relatively high CPI (6–7) and ACL (28–29) values (high %nC_{31}-alkane) and lower Paq
557 (0.2–0.1) (Fig. 5). Contrary to all previous Holocene flood layers, this is the only clastic
558 layer with higher detrital and higher lipid contents, and reflects the different nature of the
559 depositional processes. The catastrophic flash flood incorporated a much larger amount
560 of fine organic-rich sediments stored behind the dam and also from areas in the watershed
561 usually not affected by natural floods.
562 After 1959 CE the total biomarker and terrestrial biomarker concentration and long chain
563 n–alkanes decreased (high %nC_{31}-alkane) whereas the organic content increased. High
564 Paq (0.3), low CPI (4.1) and ACL (27.6) suggest higher contribution of aquatic plants
565 over terrestrial plants, consistent with a small decrease in C/N atomic ratio, and an
566 increase in lake bioproductivity (Jambrina-Enríquez et al. 2014). The human impact and
567 increased fires in the watershed from the 1990 had likely an impact on sediment and
568 nutrient delivery to the lake. Although tripernoid concentrations were low (ursolic acid

and friedelin are dominant, β-sitosterol has been not detected, probably below detection limits) (Fig. 5), their presence could reflect the documented recuperation of the *Quercus* forest during the last decades (Juliá et al. 2007) and also the higher contribution by shoreline trees as *Alnus* (Fig. 3).

Conclusions

Changes in the sedimentary n-alkane distribution and terrestrial biomarkers in Sanabria Lake sequence were driven by variable inputs from terrestrial upland plant sources in response primarily to changes in sediment delivery and watershed vegetation and secondarily to lake processes. Lipid distributions indicate a major contribution of allochthonous inputs to the sedimentary OM since deglaciation. During the proglacial stage (prior to 14.7 cal ka BP), clastic sediments with low OM content show the lowest biomarker concentration and CPI values, and indicate that the n-alkanes could have been derived from older sediment sources and older organic matter with high degree of maturity.

During the Late Glacial and the Holocene, intervals with higher biomarker concentration (high %nC_{29}, nC_{31}-alkanes) correspond to organic oozes and organic-rich silty layers. The highest CPI and ACL, and lowest Paq, the higher content of specific higher plants biomarkers and the positive relationship with long carbon chain n-alkane, n-alkanol and n-alkanoic acid content in the sediment indicate a major contribution of vascular land plants, and reflect periods of better conditions for forest development. The máximum forest development (Mid Holocene) is characterized by three intervals of higher biomarker and triterpenoids concentrations at ca. 7000–6200, 5600–5000, 4500–4000 cal BP, correlated with increasing presence of warmth-demanding taxa. Periods of lower biomarker concentration (high %nC_{27}, nC_{31}-alkanes), CPI and ACL values and higher

Paq index, reflect the synergetic effects of lower forest development in the watershed and higher dilution of the OM content in the sediment due to the greater clastic input from the Tera River (Mid Holocene events, Roman deforestation). However, during the Late Holocene, some periods of lower biomarker (nC_{23}, nC_{31}-alkanes) and triterpenoid concentrations in organic silts correspond with periods of higher lake bioproductivity (1.3–1.0 cal ka BP and from 1960 CE to recent times) and are interpreted as higher anthropic pressure in the lake system.

The integration of biomarkers and especially nalkane indices in the Sanabria sediments, geochemical and sedimentological proxies, pollen records and biomarkers from modern plants improves our reconstructions of past environmental changes and helps to evaluate the relative significance of climate and anthropogenic forcings and watershed versus lake processes.

Acknowledgments

M. Jambrina-Enríquez acknowledges support from a Ph.D. fellowship from Salamanca University (Spain) and the INTIMATE EU COST Action ES0907 in the form of a Short-Term Scientific Mission. The research has been funded by the Spanish Ministry of Science and Competitiveness (CONSOLIDER–GRACCIE Project, CSD2007-00067) and by the Fundación Patrimonio Natural de Castilla y León. We thank P. Meyers and an anonymous reviewer for helpful comments.

References

Allen JRM, Huntley B, Watts WA (1996) The vegetation and climate of northwest Iberia over the last 14,000 years. J Quat Sci 11:125–147

Bakke J, Lie Ø, Heegaard E, Dokken T, Haug GH, Birks HH, Dulski P, Nilsen T (2009) Rapid oceanic and atmospheric changes during the Younger Dryas cold period. Nat Geosci 2:202–205

Bartolomé M, Moreno A, Sancho C, Stoll HM, Cacho I, Spötl C, Belmonte A, Edwards LR, Cheng H, Hellstrom JC (2015) Hydrological change in Southern Europe responding to increasing North Atlantic overturning during Greenland Stadial 1. PNAS. doi:10.1073/pnas.1503990112

Bohn U, Gollub G, Hettwer C (2000–2003) Karte der natürlichen Vegetation Europas [map of the natural vegetation of Europe]. 1:2500000. Münster (Landwirtschaftsverlag)

Bond G, Showers W, Cheseby M, Lotti R, Almasi P, de Menocal P, Priore P, Cullen H, Hajdas I, Bonani G (1997) Pervasive millennial-scale cycle in North Atlantic Holocene and glacial climates. Science 278:1257–1266

Borruel-Abadía V, Gómez-Paccard M, Larrasoaña JC, Rico M, Valero-Garcés BL, Moreno A, Jambrina-Enríquez M, Soto R (2015) Late Pleistocene to Holocene palaeoenvironmental variability in the NW Spanish mountains: insights from a source-to-sink environmental magnetic study of Lake Sanabria. J Quat Sci 30:222–234

Brincat D, Yamada K, Ishiwatari R, Uemura H, Naraoka H (2000) Molecular-isotopic stratigraphy of long-chain n-alkanes in Lake Baikal Holocene and glacial age sediments. Org Geochem 31:287–294

644 Buggle B, Wiesenberg GL, Glaser B (2010) Is there a possibility to correct fossil n-alkane
645 data for postsedimentary alteration effects. Appl Geochem 196:86–106
646
647 Bush RT, McInerney FA (2013) Leaf wax n-alkane distributions in and across modern
648 plants: implications for paleoecology and chemotaxonomy. Geochim Cosmochim Acta
649 117:161–179
650
651 Canuel EA, Freeman KH, Wakeham SG (1997) Isotopic composition of lipid biomarker
652 compounds in estuarine plants and surface sediments. Limnol Oceanogr 42:1570–1583
653
654 Cranwell PA (1973) Chain length distribution of n-alkanes from lake sediments in
655 relation to postglacial environmental change. Freshw Biol 3:259–265
656
657 Cranwell PA, Volkman JK (1981) Alkyl and steryl esters in a recent lacustrine sediment.
658 Chem Geol 32:29–43
659
660 Cranwell PA, Eglinton G, Robinson N (1987) Lipids of aquatic organisms as potential
661 contributors to lacustrine sediments—II. Org Geochem 11:513–527
662
663 de Hoyos C (1996) Limnología del Lago de Sanabria: variabilidad interanual del
664 fitoplankton. Unpublished Ph.D. Thesis. Universidad de Salamanca
665
666 Diefendorf AF, Freeman KH, Wing SL, Graham HV (2011) Production of n-alkyl lipids
667 in living plants and implications for the geologic past. Geochim Cosmochim Acta
668 75:7472–7485

669

670 Díez-Montes A (2006) La geología del Dominio ‘‘Ollo de Sapo’’ en las comarcas de
671 Sanabria y Terra do Bolo. Ph.D. Thesis, Universidad de Salamanca

672

673 Douglas PMJ, Pagani M, Eglinton TI, Brenner M, Hodell DA, Curtis JH, Ma KF,
674 Breckenridge A (2014) Pre-aged plant waxes in tropical lake sediments and their
675 influence on the chronology of molecular paleoclimate proxy records. Geochim
676 Cosmochim Acta 141:346–364

677

678 Eglinton G, Hamilton RJ (1967) Leaf epicuticular waxes. Science 156(3780):1322–1335

679

680 Ficken KJ, Barber KE, Eglinton G (1998) Lipid biomarker, $\delta^{13}C$ and plant macrofossil
681 stratigraphy of a Scottish montane peat bog over the last two millenia. Org Geochem
682 28:217–237

683

684 Ficken KJ, Li B, Swain DL, Eglinton G (2000) An n-alkane proxy for the sedi-mentary
685 input of submerged/floating freshwater aquatic macrophytes. Org Geochem 31(7–
686 8):745–749

687

688 García P, Lauzurica P, Rey P, Roa A (1992) Informe botánico del Parque Natural del
689 Lago de Sanabria y sus Alrededores. Monografías de la red de Espacios Naturales de
690 Castilla y León. Consejería de Medio Ambiente y Ordenación del Territorio. Dirección
691 General del Medio Ambiente, Valladolid, Spain

692

693 Giralt S, Rico-Herrero MT, Vega JC, Valero-Garcés BL (2011) Quantitative climate
694 reconstruction linking meteorological, limnological and XRF core scanner datsets: the
695 Lake Sanabria case study, NW Spain. J Paleolimnol 46(3):487–502
696
697 Guijarro-Menéndez N (2012) Un pequeñoo dominio monástico en la época altomedieval:
698 El ejemplo del monasterio de San Martín de Castañeda. Territorio, Sociedad y Poder.
699 Revista de Estudios Medievales 7:63–84
700
701 Hedges JI, Prahl FG (1993) Early diagenesis: consequences for applications of molecular
702 biomarkers. In: Engel MH, Macko SA (eds) Organic geochemistry, principles and
703 applications. Plenum Press, New York, pp 237–253
704
705 Heegaard E, Birks HJB, Telford RJ (2005) Relationships between calibrated ages and
706 depth in stratigraphical sequences: an estimation procedure by mixed effect regression.
707 The Holocene 15:612–618
708
709 Hernández A, Trigo RM, Pla-Rabes S, Valero-Garcés VL, Jerez S, Rico-Herrero M, Vega
710 JC, Jambrina-Enríquez M, Giralt S (2015) Sensitivity of two Iberian lakes to North
711 Atlantic atmospheric circulation modes. Clim Dyn. doi:10.1007/ s00382-015-2547-8
712
713 Hoffmann B, Kahmen A, Cernusak LA, Arndt SK, Sachse D (2013) Abundance and
714 distribution of leaf wax n-alkanes in leaves of Acacia and Eucalyptus trees along a strong
715 humidity gradient in northern Australia. Org Geochem 62:62–67
716

Jambrina-Enríquez M, Rico M, Moreno A, Leira M, Bernárdez P, Prego R, Recio C, Valero-Garcés BL (2014) Timing of deglaciation and postglacial environmental dynamics in NW Iberia: the Sanabria Lake record. Quat Sci Rev 94:136–158

Julià R, Luque JA (2006) Climatic changes vs. catastrophic events in lacustrine systems: a geochemical approach. Quat Int 158:162–171

Julià R, Luque JA, Siera S, Alejandro JA (2007) Climatic and land use changes on the NW of Iberian Peninsula recorded in a 1500-year record from Lake Sanabria. Contrib Sci 3(3):355–369

Kawamura K, Ishiwatari R (1985) Distribution of lipid-class compounds in bottom sediments of freshwater lakes with different tropic status in Japan. Chem Geol 51:123–133

Lane CS, Brauer A, Blockley SPE, Dulski P (2013) Volcanic ash reveals time-transgressive abrupt climate change during the Younger Dryas. Geology. doi:10.1130/G34867.1

Luque JA (2003) El Lago de Sanabria: un sensor de las oscilaciones clima´ticas del Atla´ntico Norte durante los u´ltimos 6000 an˜os. Ph.D. Thesis. Universidad de Barcelona

Luque JA, Julià J (2002) Lake sediment response to land-use and climate change during the last 100 years in the oligotrophic Lake Sanabria (northwest of Iberian Peninsula). Sediment Geol 148:343–355

Mayewski PA, Rohling EJ, Stager JC, Karlèn W, Maasch KA, Meeker LD, Meyerson EA, Gasse F, Van Kreveld SA, Holmgren CA, Lee-Thorp JA, Rosqvist G, Rack F, Staubwasser M, Schneider R, Steig EJ (2004) Holocene climate variability. Quat Res 62:243–255

Mazurek MA, Simoneit BRT (1984) Characterization of biogenic and petroleum-derived organic matter in aerosols over remote, rural, and urban areas. In: Keith LH (ed) Identification and analysis of organic pollutants in air. Ann Arbor Science, Woburn, pp 353–370

Meyers PA (2003) Applications of organic geochemistry to paleoli-monological reconstructions: a summary of examples from the Laurentian Great Lakes. Org Geochem 34(2):261–289

Meyers PA, Ishiwatari R (1993) Lacustrine organic geochemistry an overview of indicators of organic matter sources and diagenesis in lake sediments. Org Geochem 20(7):867–900

Muñoz-Sobrino C, Ramil-Rego P, Gómez-Orellana L (2004) Vegetation of the Lago de Sanabria área (NW Iberia) since the end of the Pleistocene: a palaecological reconstruction on the basis of two new pollen sequences. Veg Hist Archaeobot 13:1–22

765 Muñoz-Sobrino C, Ramil-Rego P, Gómez-Orellana L (2007) Late Würm and early
766 Holocene in the mountains of northwest Iberia: biostratigraphy, chronology and tree
767 colonization. Veg Hist Archaeobot 16:223–240
768
769 Muñoz-Sobrino C, Ramil-Rego P, Gómez-Orellana L, Ferreiro da Costa J, Díaz Varela
770 RA (2009) Climatic and human effects on the post-glacial dynamics of Fagus sylvatica
771 L. in NW Iberia. Plant Ecol 203:317–340
772
773 Muñoz-Sobrino C, Heiri O, Hazekamp M, van der Velden D, Kirilova EP, García-
774 Moreiras I, Lotter AF (2013) New data on the Lateglacial period of SW Europe: a high
775 resolution multiproxy record from Laguna de la Roya (NW Iberia). Quat Sci Rev 80:58–
776 77
777
778 Ortiz JE, Gallego JLR, Torres T, Díaz-Bautista A, Sierra C (2010a) Palaeoenvironmental
779 reconstruction of Northern Spain during the last 8000 cal yr BP based on the biomarker
780 content of the Ron˜anzas peat bog (Asturias). Org Geochem 41:454–466
781
782 Ortiz JE, Torres T, Delgado A, Llamas JF, Soler V, Valle M, Moreno L, Díaz-Bautista A
783 (2010b) Palaeoenvironmental changes in the Padul Basin (Granada, Spain) over the last
784 1 Ma based on the biomarker content. Palaeogeogr Palaeoclimatol Palaeoecol 298:286–
785 299
786
787 Ortiz JE, Moreno L, Torres T, Vegas J, Ruiz-Zapata B, García-Cortés A, Galá L, Pérez-
788 González A (2013) A 220 ka palaeoenvironmental reconstruction of the Fuentillejo maar
789 lake record (Central Spain) using biomarker analysis. Org Geochem 55:85–97

Otto A, Simoneit BRT (2001) Chemosystematics and diagenesis of terpenoids in fossil conifer species and sediment from the Eocene Zeitz formation, Saxony, Germany. Geochim Cosmochim Acta 65(20):3505–3527

Rieley G, Collier RJ, Jones DM, Eglinton G (1991) The biogeochemistry of Ellesmere Lake, UK—I: source correlation of leaf wax inputs to the sedimentary record. Org Geochem 17:901–912

Rodríguez-Rodríguez L, Jiménez-Sánchez M, Domínguez-Cuesta MJ, Rico MT, Valero-Garcés BL (2011) Last deglaciation in northwestern Spain: new chronological and geomorphologic evidence from the Sanabria region. Geomorphology 135(1–2):48–65

Rontani JF, Volkman JK (2005) Lipid characterization of coastal hypersaline cyanobacterial mats from the Camargue (France). Org Geochem 36:251–272

Sachse D, Radke J, Gleixner G (2004) Hydrogen isotope ratios of recent lacustrine sedimentary n-alkanes record modern climate variability. Geochim Cosmochim Acta 68:4877–4889

Sachse D, Radke J, Gleixner G (2006) DD values of individual n-alkanes from terrestrial plants along a climatic gradient—implications for the sedimentary biomarker record. Org Geochem 37:469–483

814 Schwark L, Zink K, Lechterbeck J (2002) Reconstruction of postglacial to early Holocene
815 vegetation history in terrestrial Central Europe via cuticular lipid biomarkers and pollen
816 records from lake sediments. Geology 30(5):463–466
817
818 Shepherd T, Griffiths DW (2006) The effects of stress on plant cuticular waxes. New
819 Phytol 171:469–499
820
821 Simoneit BRT (1986) Cyclic terpenoids of the geosphere. In: Johns RB (ed) Biological
822 markers in the sedimentary record. Elsevier, Amsterdam, pp 43–99
823
824 Trigo RM, Pozo-Vázquez D, Osborne T, Castro-Díez Y, Gómiz- Fortis S, Esteban-Parra
825 MJ (2004) North Atlantic Oscillation influence on precipitation, river flow and water
826 resources in the Iberian peninsula. Int J Climatol 24:925–944
827 van Maarseveen C, Han H, Jetter R (2009) Development of the cuticular wax during
828 growth of Kalanchoe daigremontiana (Hamet et Perr. de la Bathie) leaves. Plant Cell
829 Environ 32:73–81
830
831 Vega JC, de Hoyos C, Aldasoro JJ (1992) The Sanabria Lake: the largest natural
832 freshwater lake in Spain. Limnetica 8:49–57
833
834 Vega JC, de Hoyos C, Aldasoro JJ, de Miguel J, Fraile H (2005) Nuevos datos
835 morfome´tricos para el Lago de Sanabria. Limnetica 24(1–2):115–122
836

837 Volkman JK, Barrett SM, Blackburn SI, Mansour MP, Sikes EL, Gelin F (1998)
838 Microalgal biomarkers: a review of recent research developments. Org Geochem
839 29:1163–1179
840
841 Volkman JK, Barrett SM, Blackburn SI (1999) Eustigmatophyte microalgae are potential
842 sources of C29 sterols, C22–C28 n-alcohols and C28–C32 n-alkyl diols in freshwater
843 environments. Org Geochem 30:307–318
844
845 Wang M, Zhang W, Hou J (2015) Is average chain length of plant lipids a potential proxy
846 for vegetation, environment and climate changes? Biogeosci Discuss 12:5477–5501
847
848 Zech M, Rass S, Buggle B, Löscher M, Zöller L (2012) Reconstruction of the late
849 Quaternary paleoenvironments of the Nussloch loess paleosol sequence, Germany, using
850 n-alkane biomarkers. Quat Res 78(2):226–235
851

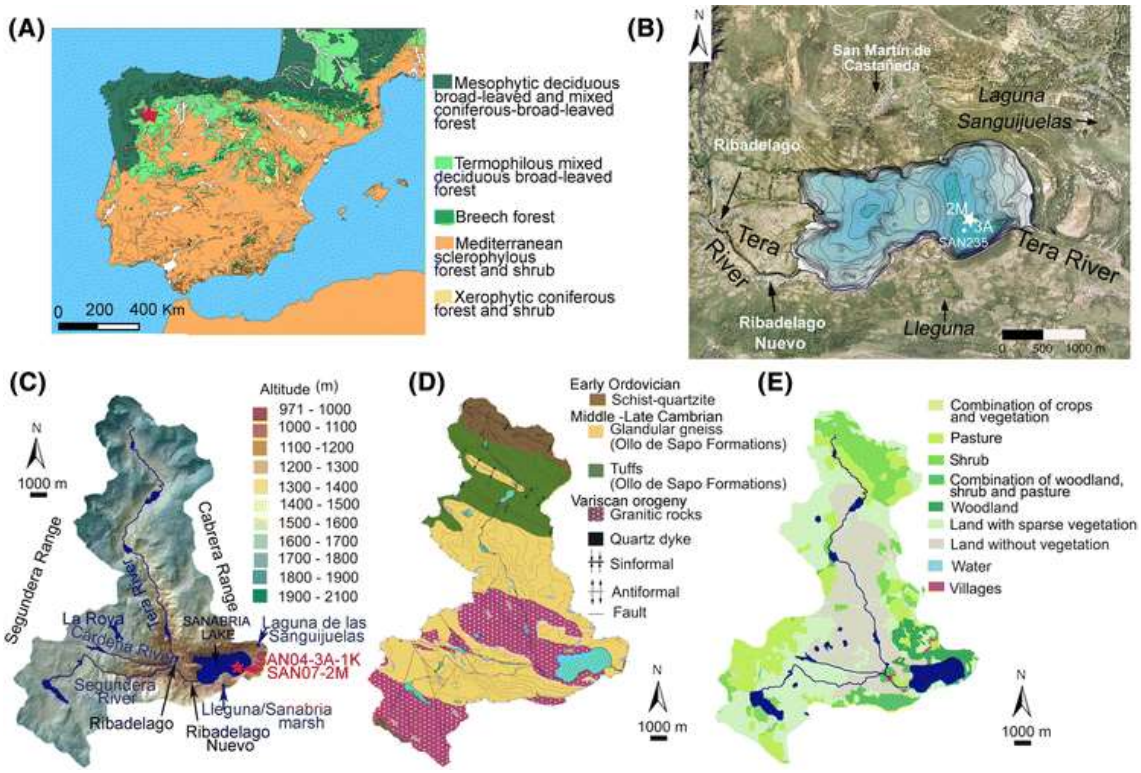

852

853 Fig. 1 **a** Vegetation biomes in Iberian Peninsula (Bohn et al. 2002, 2003); **b** bathymetric
854 map of Sanabria Lake (Vega et al. 2005) and location of the 3A (SAN07-3A-1K) and 2M
855 (SAN07-2M) cores in the eastern sub basin (Zmax = 51 m) (this study) and SAN235 core
856 (Julià et al. 2007); **c** elevation map of Sanabria Lake basin (modified from
857 www.idecyl.jcyl.es) showing the location of 3A and 2M cores (*red star*) and the nearby
858 records: *Lowlands*: Lleguna—Muñoz-Sobrino et al. 2004, previously named Sanabria
859 marsh—Allen et al. 1996, and Laguna de Sanguijuelas—Muñoz-Sobrino et al. 2004, and
860 *highlands*: Laguna La Roya (Muñoz-Sobrino et al.2013); **d** geological map (modified
861 from Díez-Montes 2006); **e** map of land use (www.ign.es)

862

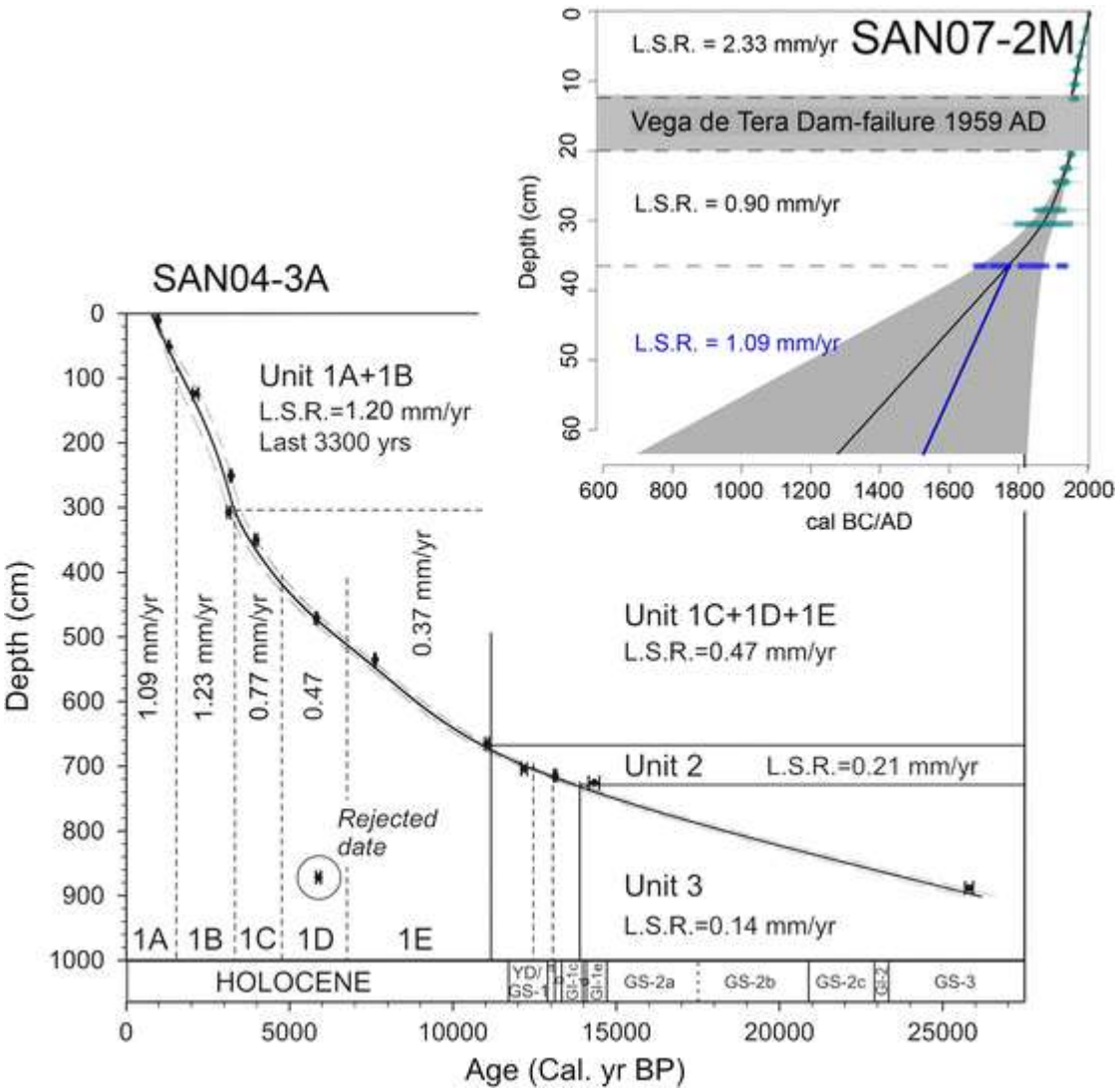

Fig. 2 Depth-age model and sedimentation rates for Sanabria sequence (from Jambrina-Enríquez et al. 2014). Chronological model for the long core SAN04-3A based on mixed effect regression function (Heegaard et al. 2005) of 13 AMS ^{14}C dates (*black dots)* and spans from 26 cal ka BP to 800 cal a BP (extrapolated age). The *continuous line* represents the age-depth function framed by dashes lines (*error lines*). Linear sedimentation rates (L.S.R.) for sedimentary units separated by *vertical dotted lines* is also indicated. The chronological model for the uppermost sediments of the Sanabria sequence (short core SAN07-2M) is based on ^{210}Pb essays (constant rate of supply model, *green horizontal line*) and 1 AMS ^{14}C data at 36.5 cm (*blue horizontal line*). The chronology of the upper 36.5 cm spans between 2005 CE and 1770 CE. The chronology for lower half (36.5–63.5 cm) was constructed using linear accumulation rates and assuming the same

874 sedimentation rate (1.09 mm $year^{-1}$) obtained for top subunit 1A in core 3A (1140-686 CE). The
875 extrapolated dates give a basal age of ca. 1520 CE
876

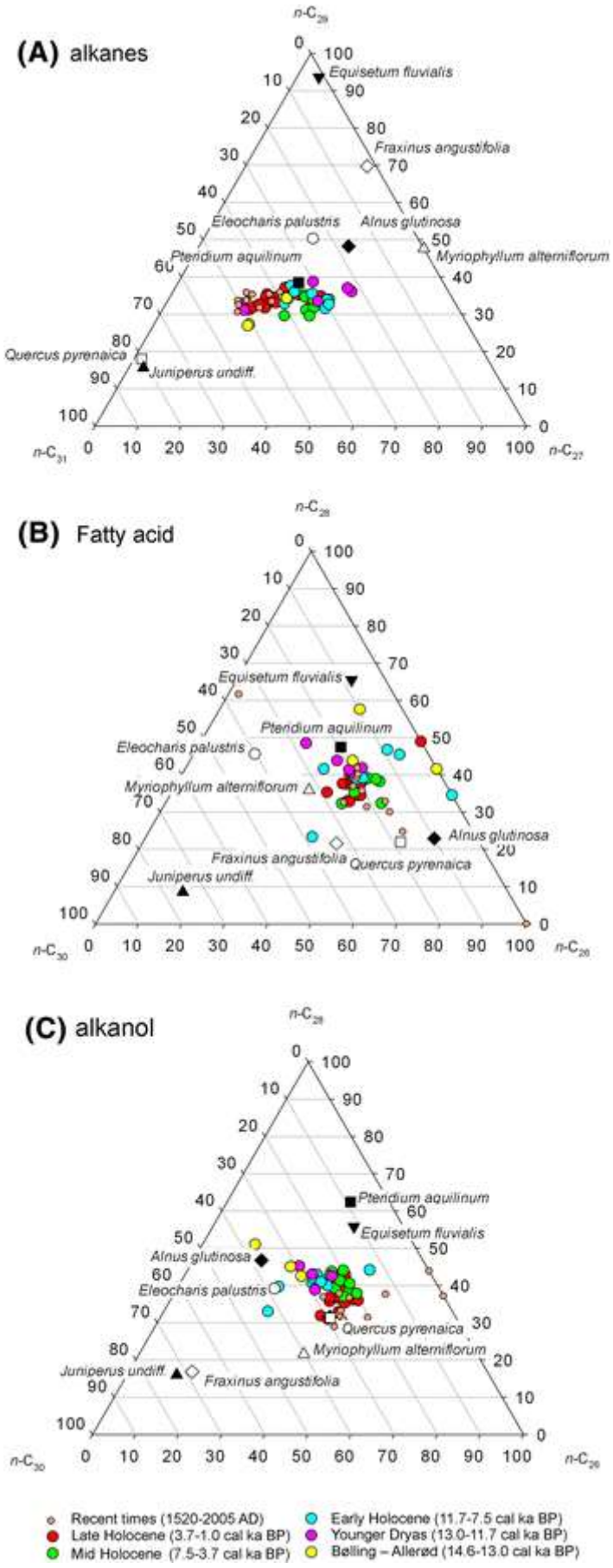
(A) alkanes
n-C29
n-C31
n-C27
Equisetum fluvialis
Fraxinus angustifolia
Eleocharis palustris
Alnus glutinosa
Pteridium aquilinum
Myriophyllum alterniflorum
Quercus pyrenaica
Juniperus undiff.
(B) Fatty acid
n-C28
n-C30
n-C26
Equisetum fluvialis
Pteridium aquilinum
Eleocharis palustris
Myriophyllum alterniflorum
Alnus glutinosa
Fraxinus angustifolia
Quercus pyrenaica
Juniperus undiff.
(C) alkanol
n-C28
n-C30
n-C26
Pteridium aquilinum
Equisetum fluvialis
Alnus glutinosa
Eleocharis palustris
Quercus pyrenaica
Myriophyllum alterniflorum
Juniperus undiff.
Fraxinus angustifolia
Recent times (1520-2005 AD)
Late Holocene (3.7-1.0 cal ka BP)
Mid Holocene (7.5-3.7 cal ka BP)
Early Holocene (11.7-7.5 cal ka BP)
Younger Dryas (13.0-11.7 cal ka BP)
Bølling – Allerød (14.6-13.0 cal ka BP)

877

878 Fig. 3 Ternary diagrams with the distribution of long-chain (**a**) *n*-alkane (nC$_{27}$, nC$_{29}$, nC$_{31}$), (**b**)
879 *n*-alkanoic acid (nC$_{26}$, nC$_{28}$, nC$_{30}$) and (**c**) *n*-alkanol (nC$_{26}$, nC$_{28}$, nC$_{30}$) in modern plants and
880 sediment samples
881

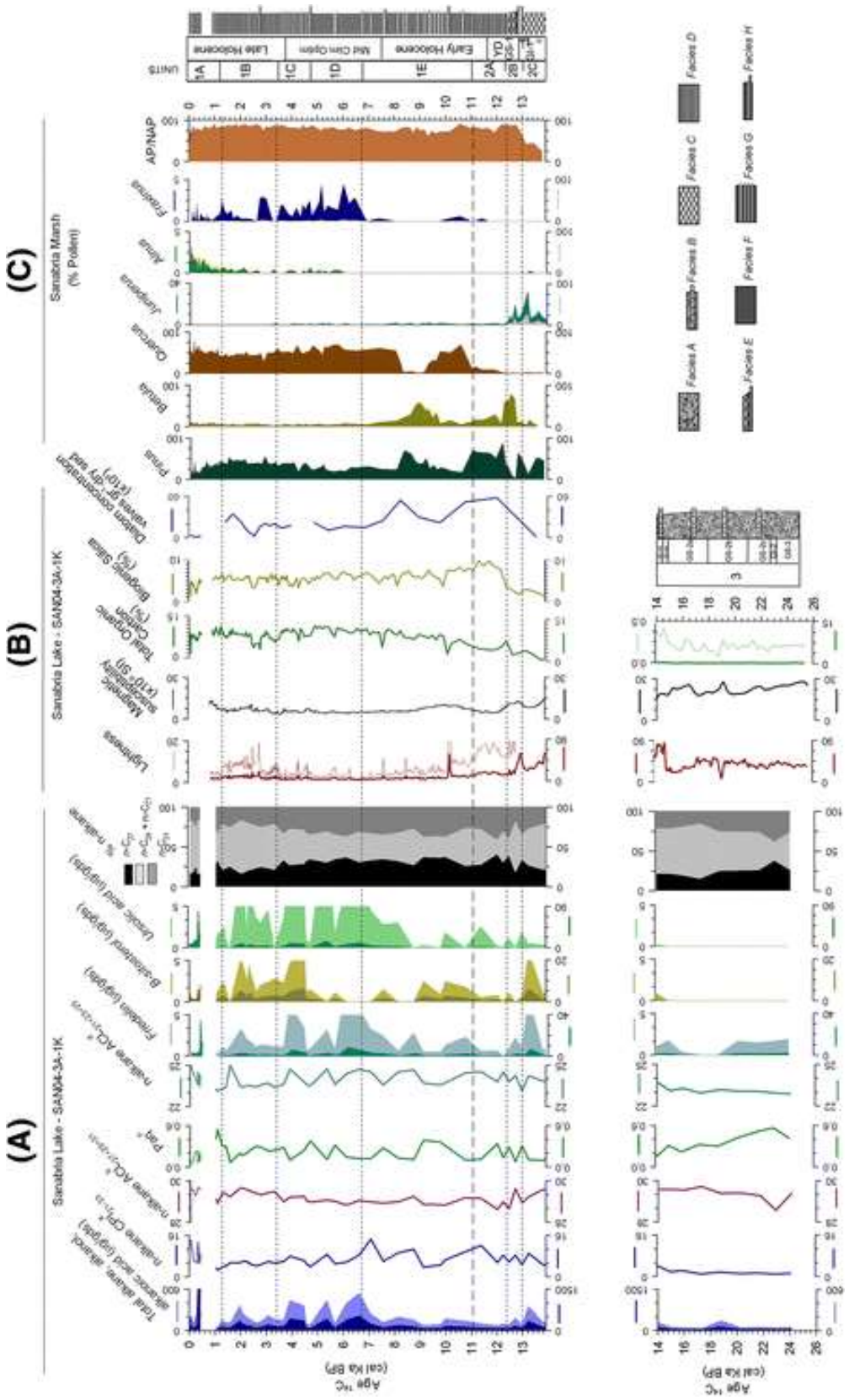

Fig. 4 Relationship of **a** biomarker components (this study), and **b** geochemical proxies (Jambrina-Enríquez et al. 2014) against extrapolated data (cores SAN04-3A and SAN07-2M); and **c** summarized pollen diagram from Sanabria marsh (Allen et al. 1996). **a** $CPI_{21–33}$-

886 $_{alkane}$:odd∑[C21–33]/even∑[C22–32], **b** $ACL_{27+29+31}$:∑(Ci * [Ci])/∑[Ci]. i = 27, 29, 31. **c**
887 P_{aq}:$(C_{23} + C_{25})/(C_{23+25+29+31})$, **d** $ACL_{21+23+25}$:∑(Ci * [Ci])/∑[Ci]. i = 21, 23, 25. Facies (further
888 details are reported by Jambrina-Enríquez et al. 2014): *Facies A* and *B*: light grey sand and silt
889 layers with the lowest organic content of the whole sequence, *Facies C*: organic dark gray silts,
890 *Facies E*: grey fine sand and fine silts, *Facies D*: faintly laminated, *very dark grayish brown*
891 organic-rich silts. *Facies F*: massive, dark organic ooze to fine organic-rich silts with intercalated
892 thin clastic layers (*Facies G*, massive silts with variable organic content and *Facies H*, sandy
893 layers with lower organic content). (Color figure online)
894

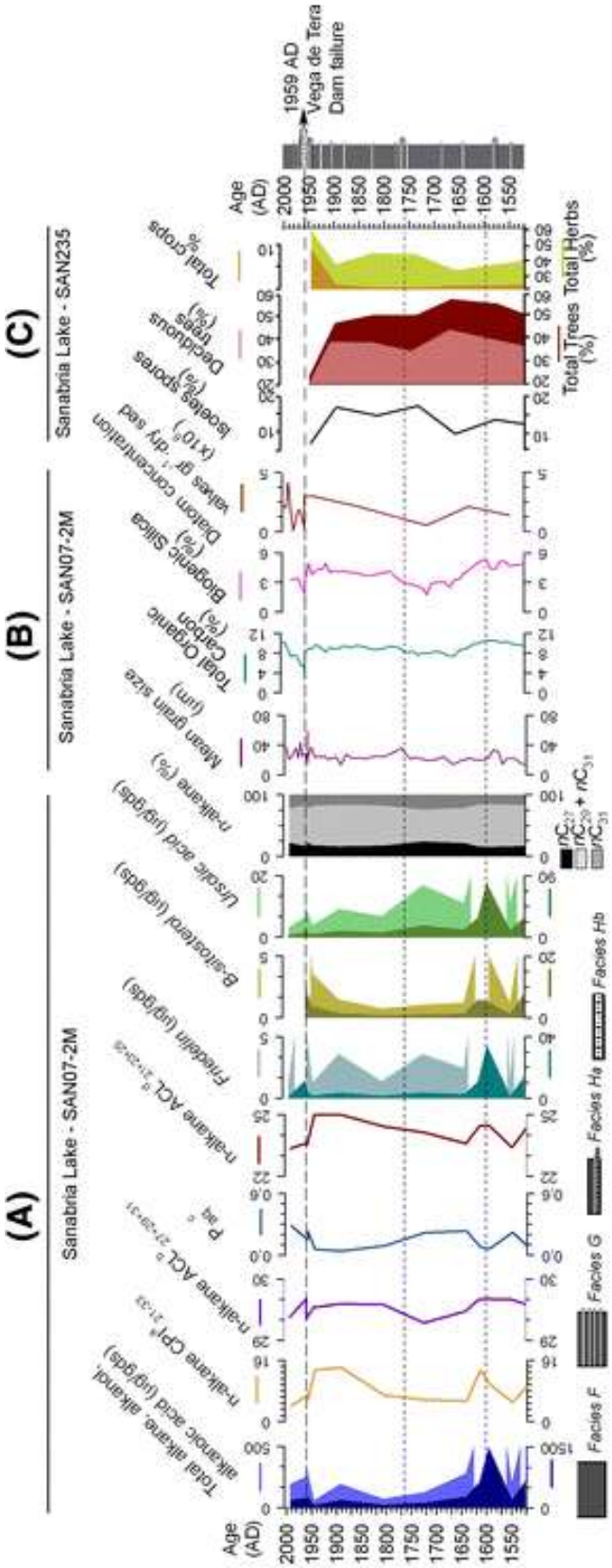

Fig. 5. The last 500 years in the Sanabria sequence. Compilation of data from core SAN07-2M: (**a**) biomarker (this study), **b** geochemical proxies (Jambrina-Enríquez et al. 2014); **c** summarized pollen diagram from Sanabria Lake (SAN235) (Julià et al.2007). **a** $CPI_{21–33\text{-alkane}}$:odd∑[C21–

899 33]/even∑[C22–32], **b** $ACL_{27+29+31}$:∑(Ci * [Ci])/∑[Ci]. i = 27, 29, 31. **c**
900 P_{aq}:(C_{23} + C_{25})/($C_{23+25+29+31}$), **d** $ACL_{21+23+25}$:∑(Ci * [Ci])/∑[Ci]. i = 21, 23, 25. Facies (further
901 details are reported by Jambrina-Enríquez et al. 2014): Facies F: massive, dark organic ooze to
902 fine organic-rich silts with intercalated thin clastic layers (Facies G, massive silts with variable
903 organic content; Facies Ha, sandy layers with lower organic content and Facies Hb, prominent
904 coarse-grained layer deposited after the Tera River Dam failure in 1959 CE)
905

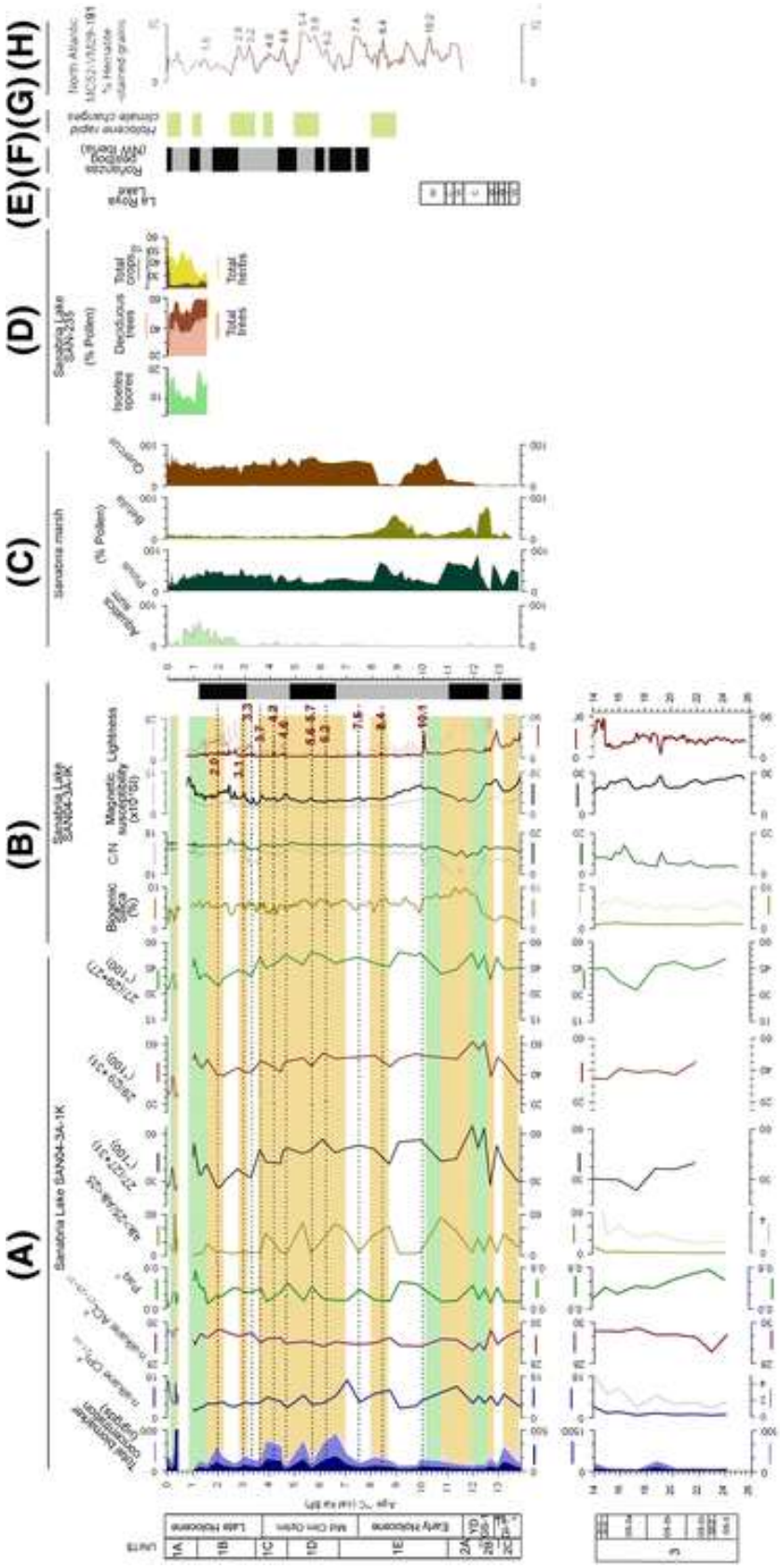

906

907 Fig. 6 Comparison of the Sanabria biomarker records with local and regional

908 palaeoenvironmental reconstructions since deglaciation. **a** Total biomarker concentration, *n*-

alkane-CPI and ACL, P_{aq}, Alk > C25/Alk < C25 and long-chain n-alkane ratios [LARs: C27/(C27 + C31), C29/(C31 + C29), C27/(C27 + C29)] **a** $CPI_{21–33\text{-alkane}}$:odd∑[C21–33]/even∑[C22–32], **b** $ACL_{27+29+31}$:∑(Ci * [Ci])/∑[Ci]. i = 27, 29, 31. **c** P_{aq}:(C_{23} + C_{25})/($C_{23+25+29+31}$). The *brown bands* indicate warmer (a may be wetter) periods and more forested watershed. The *green band* indicates higher bioproductivity periods; **b** compilation of sedimentological and geochemical data from 3A and 2M cores, and main humid (*grey*) and dry (*black*) episodes (Jambrina-Enríquez et al. 2014); **c** summarized pollen diagram from Sanabria marsh (Allen et al. 1996) also known as Lleguna site (Muñoz-Sobrino et al.2004); **d** summarized pollen diagram from Sanabria Lake (the last 1500 years, SAN-235) (Julià et al. 2007); **e** Chironomid-inferred July air temperatures from La Roya Lake (Muñoz-Sobrino et al. 2013)—*w* warm, *c* cold; (F) Humid (*grey*) and dry (*black*) episodes based on the biomarker content from Roñanzas peatbog (Ortiz et al. 2010a); **g** Holocene rapid climate changes from Mayewski et al. 2004; **h** hematite stained grains percentage (%HSG) at North Atlantic core VM 29-191 (Bond et al.1997)

ESM1. Description of sediment samples (depth, extrapolated age), *n*-alkane distribution in terms of range of chain lenght (C range), Most abundant (C max), Total alkane concentration (µg per gram of dry sample - µg gds^{-1}), Carbon preference index (CPI), proportion of aquatic plants (Paq), Average chain length (ACL). Total lipid concentration (*n*-alkane, *n*-alkanol and *n*-alkanoic acid) (µg gds^{-1}), higher plants biomarkers (Friedelin, B-sitosterol and ursolic acid) (µg gds^{-1}). (a) CPI21-33: odd∑[C21-33]/even∑[C22-32], (b) Paq: (C23+C25)/(C23+25+29+31), (c) ACL21-33:∑ (Ci*[Ci])/∑[Ci]. 21<i<33

SAN07-2M - *n*-alkanes														
Unit	Depth (cm)	Age (AD)	*C range*	*C max*	Total Alkanes (µg gds^{-1})	$nC_{21}+nC_{23}+nC_{25}$	$nC_{27}+nC_{29}+nC_{31}$	CPI^{a}_{21-33}	Paq^{b}	ACL^{c}_{21-33}	Total Lipid (µg gds^{-1})	Friedelin (µg gds^{-1})	B-sitosterol (µg gds^{-1})	Ursolic acid (µg gds^{-1})
	3.5	1990	C_{21}-C_{31}	C_{31}	22.1	4.5	11.9	4.1	0.3	27.6	191.1	1.2	-	3.2
Vega de Tera Dam failure	13.5	1959	C_{21}-C_{31}	C_{31}	42.7	4.6	27.0	7.0	0.1	29.2	256.8	11.7	14.1	6.5
	18.5	1959	C_{21}-C_{31}	C_{31}	44.5	7.6	27.4	5.7	0.2	28.1	309.4	6.1	9.8	10.1
	21.5	1950	C_{25}-C_{31}	C_{31}	8.9	0.4	7.4	13.5	0.1	29.3	61.0	1.3	3.6	3.8
	28.5	1890	C_{25}-C_{31}	C_{31}	17.5	0.5	14.1	14.0	0.0	29.8	193.7	3.6	1.5	9.1
	34.5	1810	C_{22}-C_{31}	C_{31}	9.5	0.6	7.1	6.8	0.1	29.1	72.3	1.4	0.7	6.8
	41.5	1720	C_{22}-C_{31}	C_{31}	23.2	3.2	15.5	5.7	0.2	28.1	125.0	3.6	1.0	16.8
	50.5	1640	C_{21}-C_{31}	C_{31}	36.6	6.2	22.1	5.4	0.2	28.2	277.6	2.4	1.2	11.0
	53.5	1610	C_{23}-C_{31}	C_{31}	117.9	6.1	90.7	13.5	0.1	29.7	646.1	10.7	5.9	28.0
	55.5	1600	C_{22}-C_{31}	C_{31}	266.2	10.8	197.5	9.8	0.1	29.7	1497.3	34.2	5.4	79.5
	60.5	1550	C_{21}-C_{31}	C_{31}	24.9	4.2	14.3	5.0	0.2	28.3	199.4	1.4	1.2	10.8
	63.5	1520	C_{23}-C_{31}	C_{31}	132.1	8.3	97.0	9.0	0.1	29.5	673.8	13.7	7.7	27.9
SAN04-3A-1K- n-alkanes														
Unit		Depth (cm)	Age (cal a BP)	*C range*	*C max*	Total Alkanes (µg.gds^{-1})	$nC_{21}+nC_{23}+nC_{25}$	$nC_{27}+nC_{29}+nC_{31}$	CPI^{a}_{21-33}	Paq^{b}	ACL^{c}_{21-33}	Total Lipid (µg gds^{-1})	Friedelin (µg gds^{-1})	B-sitosterol (µg gds^{-1})	Ursolic acid (µg gds^{-1})
1	A	27	1000	C_{21}-C_{31}	$C_{29}+C_{31}$	6.7	1.9	3.2	3.4	0.4	26.3	56.7	0.5	0.8	0.8
		32	1100	C_{21}-C_{31}	C_{23}	5.9	2.1	2.1	2.5	0.5	25.4	51.9	0.2	1.3	1.6
	B	52	1300	C_{21}-C_{33}	C_{31}	11.4	2.6	5.9	3.7	0.3	27.2	153.4	1.0	2.3	2.2
		62	1400	C_{21}-C_{33}	C_{31}	13.5	2.9	7.4	4.2	0.3	27.4	124.3	1.0	2.2	2.6
		67	1500	C_{21}-C_{33}	C_{31}	17.2	3.7	9.4	4.1	0.3	27.4	121.1	0.6	1.4	1.0
		83	1600	C_{22}-C_{33}	$C_{29+}C_{31}$	23.7	0.9	17.5	5.4	0.1	28.8	103.2	1.3	-	-
		122	2000	C_{21}-C_{33}	C_{31}	57.8	8.7	34.6	5.3	0.2	28.5	366.8	3.2	5.0	8.8
		132	2100	C_{21}-C_{33}	C_{31}	31.4	4.2	19.7	6.0	0.2	28.6	257.2	3.1	4.7	9.3
		152	2200	C_{21}-C_{33}	C_{31}	25.9	4.1	16.1	5.9	0.2	28.4	189.4	1.9	2.5	2.0

		157	2300	C_{21}-C_{33}	C_{31}	24.3	4.1	14.5	5.1	0.2	28.1	181.5	2.0	4.4	7.7
		192	2600	C_{21}-C_{33}	C_{31}	11.3	2.4	6.2	4.1	0.3	27.4	111.9	1.1	1.2	3.7
		217	2800	C_{21}-C_{33}	C_{31}	15.2	3.0	8.7	4.7	0.3	27.6	132.2	1.4	2.1	3.1
		262	3100	C_{21}-C_{33}	C_{31}	26.3	4.3	16.3	5.8	0.2	28.3	219.8	1.3	2.4	4.5
	C	302	3300	C_{21}-C_{33}	C_{31}	24.2	4.4	13.9	5.2	0.2	28.1	160.5	1.1	2.8	-
		339	3700	C_{21}-C_{33}	$C_{27+}C_{31}$	24.0	4.8	14.7	5.8	0.3	27.6	149.9	1.1	2.3	3.5
		359	3900	C_{22}-C_{33}	C_{31}	56.3	3.5	43.4	7.9	0.1	29.0	435.9	6.3	4.7	9.8
		399	4500	C_{21}-C_{33}	C_{31}	38.4	6.4	24.4	6.2	0.2	28.1	357.7	3.4	6.3	8.3
		409	4600	C_{21}-C_{33}	$C_{27+}C_{31}$	16.0	3.2	9.4	5.0	0.3	27.5	96.5	0.8	1.4	1.0
		414	4700	C_{21}-C_{33}	$C_{27+}C_{31}$	17.1	4.1	8.9	3.9	0.4	26.9	91.3	0.9	1.5	0.6
	D	449	5400	C_{22}-C_{33}	C_{29}	58.8	7.2	82.5	8.7	0.1	28.9	437.9	3.2	-	14.9
		464	5700	C_{21}-C_{33}	$C_{27+}C_{31}$	15.7	3.3	9.1	5.0	0.3	27.4	103.4	0.9	1.1	1.9
		484	6100	C_{21}-C_{33}	C_{27}	34.3	2.9	24.9	5.6	0.1	28.4	393.1	8.8	-	7.3
		505	6600	C_{23}-C_{33}	$C_{29+}C_{31}$	66.3	4.9	51.4	8.4	0.1	28.8	542.7	5.6	-	10.9
	E	523	7100	C_{21}-C_{33}	$C_{27+}C_{29}$	33.6	2.6	27.4	14.5	0.1	28.7	241.4	3.3	-	4.6
		543	7600	C_{21}-C_{33}	C_{27}	27.4	5.3	17.0	5.9	0.3	27.6	117.5	2.5	1.5	2.8
		568	8200	C_{21}-C_{33}	C_{29}	64.0	5.2	49.8	9.2	0.1	28.7	195.5	0.6	-	3.0
		593	8800	C_{22}-C_{33}	C_{31}	45.0	3.1	35.3	10.6	0.1	29.1	154.4	2.8	-	-
		608	9100	C_{21}-C_{33}	C_{27}	18.7	4.4	9.6	3.6	0.4	27.0	75.9	0.5	2.5	0.3
		632	9800	C_{21}-C_{33}	C_{27}	23.5	5.4	12.9	4.5	0.4	27.1	85.8	0.5	0.9	-
		638	10000	C_{21}-C_{33}	C_{27}	27.8	5.6	17.3	6.5	0.3	27.6	170.8	1.3	2.5	1.9
		662	10800	C_{23}-C_{33}	C_{29}	59.3	3.7	46.3	9.7	0.1	29.1	136.6	2.3	1.8	-
2	A	678	11400	C_{23}-C_{33}	$C_{29+}C_{31}$	58.2	4.1	45.1	12.1	0.1	29.1	100.2	0.6	0.5	2.6
		693	12000	C_{21}-C_{33}	C_{27}	17.1	3.5	10.3	5.5	0.3	27.3	74.8	0.7	0.8	0.2
		698	12200	C_{23}-C_{33}	C_{29}	18.7	1.5	14.0	8.2	0.1	28.7	92.2	-	-	0.1
	B	703	12500	C_{21}-C_{33}	C_{27}	21.8	3.9	13.7	5.7	0.3	27.5	87.9	1.0	1.1	1.2
		708	12700	C_{21}-C_{33}	C_{31}	59.8	3.1	41.7	8.3	0.1	29.7	182.4	2.3	-	-
		713	13000	C_{21}-C_{33}	C_{27}	20.6	4.5	10.8	4.6	0.3	27.5	90.5	1.0	0.7	1.9
	C	718	13200	C_{21}-C_{33}	C_{31}	77.1	5.3	55.5	9.1	0.1	29.2	352.0	7.2	6.1	0.5
		728	13800	C_{21}-C_{33}	C_{31}	42.9	2.6	26.3	4.7	0.1	29.4	128.2	0.8	1.2	0.4
3		749	15000	C_{21}-C_{33}	C_{31}	14.0	2.4	5.0	1.8	0.3	27.5	49.9	1.8	-	-
		764	16000	C_{21}-C_{33}	C_{31}	7.4	1.0	3.5	2.2	0.2	28.0	42.8	0.4	-	-

		784	17300	C_{21}-C_{33}	C_{31}	4.9	0.8	1.4	0.9	0.3	26.9	36.1	-	-	-
		804	18800	C_{21}-C_{33}	C_{31}	16.3	2.7	6.3	1.7	0.3	27.4	64.4	-	-	-
		824	20200	C_{21}-C_{33}	C_{22}	15.1	2.8	3.9	1.1	0.4	26.8	45.1	1.7	-	-
		844	21800	C_{21}-C_{33}	C_{22}	21.2	5.6	5.4	1.3	0.5	26.0	48.7	1.5	-	-
		859	23000	C_{21}-C_{33}	C_{22}	12.8	2.8	2.4	0.9	0.6	26.2	42.8	1.7	-	-
		874	24100	C_{21}-C_{33}	C_{22}	11.7	2.5	3.1	1.2	0.4	26.4	44.1	1.9	-	-

ESM2. Description of sediment samples (depth, extrapolated age), *n*-alkanol and *n*-alkanoic acid distribution in terms of range of chain leng (C range), most abundant (C max), total alkanol and alkanoic acid concentration (µg per gram of dry sample - µg gds^{-1}), carbon preference index (CPI). (a) CPI20-34:even∑[C20-34]/odd∑[C21-33], (b) CPI16-32:even∑[C16-32]/odd ∑[C21-31].

SAN-07-2M *n*-alkanol and *n*-alkanoic acid										
Unit	Depth (cm)	Age (AD)	C range	C max	Total Alkanol (µg gds^{-1})	CPI^a_{20-33}	C range	C max	Total Alkanoic acid (µg gds^{-1})	CPI^b_{16-32}
	3.5	1990	C_{20}-C_{33}	C_{28}	64.8	6.7	C_{16}-C_{32}	C_{26}	104.2	4.2
Vega de Tera Dam failure	13.5	1959	C_{20}-C_{32}	C_{26}	90.6	7.7	C_{16}-C_{32}	$C_{24+}C_{26}$	123.5	3.4
	18.5	1959	C_{20}-C_{32}	C_{26}	114.4	5.8	C_{16}-C_{32}	C_{24}	150.5	5.6
	21.5	1950	C_{20}-C_{32}	C_{26}	35.5	21.7	C_{18}-C_{26}	C_{24}	16.5	4.2
	28.5	1890	C_{20}-C_{32}	C_{26}	99.8	13.2	C_{16}-C_{30}	C_{26}	76.3	4.2
	34.5	1810	C_{20}-C_{32}	C_{26}	47.9	26.7	C_{20}-C_{30}	C_{24}	14.8	2.8
	41.5	1720	C_{20}-C_{32}	C_{26}	67.9	13.1	C_{18}-C_{30}	C_{26}	33.8	16.5
	50.5	1640	C_{20}-C_{32}	C_{26}	92.5	10.1	C_{16}-C_{32}	$C_{24+}C_{26}$	148.5	3.4
	53.5	1610	C_{20}-C_{32}	C_{26}	253.3	7.9	C_{16}-C_{32}	C_{28}	274.9	3.5
	55.5	1600	C_{20}-C_{32}	C_{26}	584.4	0.1	C_{16}-C_{32}	C_{28}	641.6	4.1
	60.5	1550	C_{20}-C_{32}	C_{26}	61.0	7.0	C_{16}-C_{32}	C_{24}	113.6	3.8
	63.5	1520	C_{20}-C_{32}	C_{26}	285.1	8.5	C_{16}-C_{32}	C_{28}	256.6	5.5

SAN-04-3A-1K *n*-alkanol and *n*-alkanoic acid											
Unit		Depth (cm)	Age (cal a BP)	C range	C max	Total Alkanol (µg gds^{-1})	CPI^a_{20-34}	C range	C max	Total Alkanoic acid (µg gds^{-1})	CPI^b_{16-32}
1	A	27	1000	C_{20}-C_{32}	C_{26}	21.8	6.7	C_{16}-C_{32}	C_{24}	28.3	6.1
		32	1100	C_{20}-C_{32}	C_{26}	9.0	10.2	C_{16}-C_{32}	C_{24}	37.1	7.0
	B	52	1300	C_{20}-C_{32}	C_{28}	56.1	23.4	C_{16}-C_{32}	C_{26}	85.9	5.4
		62	1400	C_{20}-C_{32}	C_{26}	48.2	24.0	C_{16}-C_{32}	C_{26}	62.7	7.5
		67	1500	C_{20}-C_{34}	C_{26}	53.3	9.3	C_{16}-C_{32}	C_{26}	50.5	5.9
		83	1600	C_{20}-C_{32}	C_{28}	54.7	14.5	C_{16}-C_{28}	C_{24}	24.9	3.0
		122	2000	C_{20}-C_{34}	C_{26}	124.6	13.1	C_{16}-C_{32}	C_{26}	184.4	6.6
		132	2100	C_{20}-C_{34}	C_{26}	102.1	7.9	C_{16}-C_{32}	C_{26}	123.7	4.3
		152	2200	C_{20}-C_{34}	C_{26}	73.4	9.1	C_{16}-C_{32}	C_{26}	90.1	5.2
		157	2300	C_{20}-C_{34}	C_{26}	62.5	16.2	C_{16}-C_{32}	$C_{26+}C_{28}$	94.8	5.2
		192	2600	C_{20}-C_{32}	C_{26}	44.8	18.6	C_{16}-C_{32}	C_{26}	55.9	6.3
		217	2800	C_{20}-C_{32}	$C_{26+}C_{28}$	51.3	14.9	C_{16}-C_{32}	C_{26}	65.7	7.4
		262	3100	C_{20}-C_{34}	$C_{26+}C_{28}$	80.2	14.2	C_{16}-C_{32}	C_{26}	113.2	6.4
	C	302	3300	C_{20}-C_{32}	C_{26}	73.9	5.2	C_{16}-C_{32}	C_{24}	62.5	3.8
		339	3700	C_{20}-C_{34}	C_{28}	63.9	17.0	C_{16}-C_{32}	$C_{26+}C_{28}$	62.1	5.7
		359	3900	C_{20}-C_{32}	C_{26}	306.0	9.1	C_{16}-C_{30}	C_{26}	73.6	4.3
		399	4500	C_{20}-C_{34}	C_{26}	142.8	8.9	C_{16}-C_{32}	C_{26}	176.6	6.1
		409	4600	C_{20}-C_{32}	C_{28}	36.9	25.4	C_{16}-C_{32}	$C_{26+}C_{28}$	43.6	7.3
		414	4700	C_{20}-C_{32}	C_{28}	32.8	24.9	C_{16}-C_{30}	C_{26}	41.5	8.0
	D	449	5400	C_{20}-C_{32}	C_{26}	128.1	7.0	C_{16}-C_{30}	C_{26}	204.1	5.4
		464	5700	C_{20}-C_{32}	C_{26}	43.4	7.6	C_{16}-C_{30}	C_{26}	44.2	9.1
		484	6100	C_{22}-C_{32}	C_{28}	322.0	6.6	C_{16}-C_{30}	C_{26}	36.8	5.6
		505	6600	C_{20}-C_{32}	C_{28}	319.0	7.4	C_{16}-C_{32}	$C_{26+}C_{28}$	157.5	3.2
	E	523	7100	C_{20}-C_{32}	C_{28}	141.7	8.50	C_{16}-C_{30}	C_{26}	66.1	7.2
		543	7600	C_{20}-C_{32}	C_{28}	37.5	5.20	C_{16}-C_{32}	C_{28}	52.6	6.7
		568	8200	C_{22}-C_{32}	C_{28}	72.5	8.80	C_{16}-C_{30}	C_{28}	59.0	13.5
		593	8800	C_{22}-C_{32}	C_{30}	86.8	4.00	C_{16}-C_{30}	C_{26}	22.6	11.8

		608	9100	C_{20}-C_{32}	C_{30}	27.0	4.90		C_{16}-C_{32}	C_{26}	30.1	5.7
		632	9800	C_{20}-C_{32}	C_{28}	23.6	14.0		C_{16}-C_{32}	C_{26}	38.7	7.7
		638	10000	C_{20}-C_{32}	C_{28}	55.9	9.9		C_{16}-C_{32}	C_{26}	87.1	7.2
		662	10800	C_{22}-C_{32}	C_{28}	63.9	4.7		C_{18}-C_{28}	C_{24}	13.4	2.0
2	A	678	11400	C_{22}-C_{32}	C_{28}	11	5.2		C_{16}-C_{31}	C_{26}	31	4.1
		693	12000	C_{20}-C_{32}	C_{28}	23.4	47.3		C_{16}-C_{32}	$C_{26+}C_{28}$	34.3	9.6
		698	12200	C_{22}-C_{32}	C_{28}	65.7	6.5		C_{16}-C_{30}	C_{28}	7.8	13.0
	B	703	12500	C_{20}-C_{32}	C_{28}	28	15.5		C_{16}-C_{32}	C_{28}	38.2	7.8
		708	12700	C_{20}-C_{32}	C_{28}	110.2	8.0		C_{16}-C_{31}	C_{24}	12.5	2.5
		713	13000	C_{20}-C_{32}	C_{28}	27.7	11.2		C_{16}-C_{32}	C_{28}	42.2	5.3
	C	718	13200	C_{20}-C_{32}	C_{28}	234.4	7.4		C_{16}-C_{30}	C_{28}	40.5	6.0
		728	13800	C_{22}-C_{32}	C_{28}	76	7.6		C_{16}-C_{30}	C_{28}	9.3	6.3
3		749	15000	C_{20}-C_{32}	C_{28}	26.4	24.9		C_{20}-C_{29}	C_{22}	9.50	1.000
		764	16000	C_{20}-C_{32}	C_{28}	25.5	52.1		C_{21}-C_{28}	$C_{22+}C_{24}$	10.00	1.000
		784	17300	C_{20}-C_{32}	C_{28}	25	43.1		C_{21}-C_{27}	$C_{22+}C_{25}$	6.20	1.000
		804	18800	C_{20}-C_{32}	C_{28}	35.5	12.2		C_{21}-C_{29}	$C_{22+}C_{24}$	12.60	0.800
		824	20200	C_{20}-C_{32}	C_{28}	22.2	55.9		C_{21}-C_{29}	$C_{22+}C_{24}$	7.70	0.900
		844	21800	C_{20}-C_{32}	C_{28}	18.7	-		C_{22}-C_{29}	$C_{22+}C_{24}$	8.90	1.000
		859	23000	C_{20}-C_{32}	C_{28}	21.2	80.4		C_{22}-C_{29}	$C_{22+}C_{24}$	8.70	1.000
		874	24100	C_{20}-C_{32}	C_{28}	22.3	69.1		C_{22}-C_{30}	$C_{22+}C_{27}$	10.00	1.200